EPJ manuscript No.
(will be inserted by the editor)

Deformation of a tethered polymer in uniform flow

Roland Rzehak[1,3,4], Wolfgang Kromen[1], Toshihiro Kawakatsu[2,3] and Walter Zimmermann[1,3,4]

[1] FORUM Modellierung and Inst. für Festkörperforschung, Forschungszentrum Jülich, D-52425 Jülich, Germany
[2] Dept. of Computational Science and Eng., Nagoya University, Furo-cho, Chikusa-ku, Nagoya 464-8603, Japan
[3] Max–Planck–Institute for Physics of Complex Systems, Nöthnitzer Str. 38, D-01187 Dresden, Germany
[4] Theoretische Physik, Universität des Saarlandes, D-66041 Saarbrücken, Germany

the date of receipt and acceptance should be inserted later

Abstract. Static properties of a single polymer fixed at one end and subjected to a uniform flow field are investigated for several polymer models: the Gaussian chain, the freely jointed chain and the FENE (**F**inite **E**xtensible **N**onlinear **E**lastic) chain. By taking into account first the excluded volume interaction and subsequently also the hydrodynamic interaction the polymer models are gradually completed and the relevance of each effect for the polymer deformation can be identified. Results from computer simulations of these bead spring chains are compared with analytical calculations using either the conformational distribution–function or blob models. To this end in contrast to the blob model with non–draining blobs introduced for a tethered polymer by Brochard-Wyart we here develop also a model with free–draining blobs. It turns out that a limited extensibility of the polymer – described by nonlinear spring forces in the model – leads to a flow velocity dependence of the end–to–end distance, segment density etc. which agrees with the power law predictions of the blob model only for very long chains and in a narrow range of flow velocities. This result is important for comparison with recent experiments on DNA molecules which turn out to be still rather short in this respect. The relative importance of finite extensibility, the excluded volume effect and hydrodynamic interactions for polymers in flow is not fully understood at present. The simulation of reasonably long chains becomes possible even when fluctuating hydrodynamic interactions are taken into account without employing averaging procedures by introducing efficient approximation schemes. At medium velocity of the uniform flow the polymer is partially uncoiled and simulations show that the effects of excluded volume and hydrodynamic interactions are position dependent. Both are stronger near the free end than near the tethered end of the polymer. A crossover from a nearly non–draining polymer at small flow velocities to a free–draining almost uncoiled chain at large velocities is found in the simulations. Accordingly, models assuming the polymer to be composed of either free- or non–draining subunits, like the two blob models, cannot correctly describe the extension and shape of a tethered polymer in flow and simple power laws for the polymer extension etc. cannot be expected.

PACS. 83.10.Nn Polymer Dynamics – 83.20.Di Microscopic Theories – 83.20.Jp Computer Simulation – 36.20.Ey Conformation

1 Introduction

The deformation of flexible polymers in flow causes the non–Newtonian fluid behavior of dilute polymer solutions which has been of both theoretical and practical interest already for a long time [1–7]. Non–Newtonian flow phenomena [8] are often puzzling like rod climbing and the secondary flows occurring in various geometries. Sometimes they are outrightly spectacular like the effect of turbulent drag reduction [9–13]. They are at the heart of important technological processes such as fiber spinning and film blowing and they are successfully applied *e.g.* for viscosity enhancement in secondary oil recovery. However, a generally accepted theoretical basis for the description of the large scale motion of non-Newtonian fluids similar to the Navier–Stokes equation for simple fluids like water is not available yet.

As for the description of simple fluids [14–16] also for polymeric liquids, the basis of a macroscopic theory are conservation laws and the laws of thermodynamics [1,3, 17,18]. But it is generally agreed upon that the deformation of the polymer molecules by the surrounding flow is crucial for the rheology of dilute polymer solutions [19–22]. Hence for polymer solutions the usual equations for the solvent have to be coupled with additional equations describing the deformation and the dynamics of the dissolved polymers. However, at present this has been achieved only for special cases.

A quantitative analysis of the polymer–flow interaction causing the deformation of the polymer has been hampered by two difficulties. On the experimental side the

classic measurement techniques such as light scattering [23], birefringence [24,25], rheometry [26,27] and small angle neutron scattering [28] provide only volume averaged quantities from which only little can be deduced about the interplay between the flow field and the individual polymers. On the theoretical side the large number of polymer degrees of freedom which are coupled by various nonlinear interactions makes a treatment of the polymer–flow interaction on a fundamental level a formidable task.

To facilitate a calculation of the polymer deformation simplified approaches have been proposed. The Rouse–Zimm model [29–32] uses a description of the polymer dynamics which is linearized about the equilibrium state and thus is questionable in strong flows. It provides the basis of the upper convected Maxwell model [33]. In the case of two beads only, *i.e.* for the dumbbell, this is also known as the Oldroyd–B–model which gives a good description only of a restricted class of substances, the so-called Boger fluids [17]. The restricted applicability of this constitutive model must be attributed to the approximations of the Rouse–Zimm model. The upper convected Maxwell model reduces to the "linear viscoelastic model" (Maxwell model) for incompressible viscoelastic fluids when the total strain is small [1,3,17,32]. Under this restriction on the flow the "linear viscoelastic model" is generally accepted as a valid description for arbitrary substances. In this linear regime there are also standard rheological techniques available for determining the frequency dependent viscosity appearing in the model. When linear disturbances are sufficient, this approach is able to predict *e.g.* pattern formation in vertically vibrated layers of viscoelastic fluids (Faraday instability) [34].

Beyond the linear regime only rather qualitative ideas about the polymer–flow interaction exist. For instance it has been shown that only flows where the elongational component dominates vorticity possess the ability to induce strong deformations of polymers [35]. It is then important to capture the nonlinear elasticity of the polymer which leads to a saturation of the polymer deformation at large elongation rates. Whether the polymer is actually deformed depends on the ratio of its longest relaxation time to the time scale set by the velocity gradient of the flow [36]. Due to conformation dependent hydrodynamic interactions the relaxation time is expected to be larger in the stretched state resulting in hysteretic behavior [19]. These ideas have been used to argue for a truncation of the turbulent cascade as a qualitative explanation of the drag reduction phenomenon [37]. To obtain quantitative rheological predictions in simpler flows a phenomenological dumbbell model has been proposed as a kind of minimal model for an extensible object [17,22,33,38]. However, these qualitative ideas are not undisputed let alone their quantitative expression. Furthermore the neglect of the many degrees of freedom of the polymer has not been justified and its consequences are unknown.

A precise experimental observation of the deformation of a single polymer by flows has become possible only very recently. For instance, the experimental work on single tethered DNA molecules in uniform flow [39,40] gives detailed data about the global extension as well as the shape of the polymer. This new approach for measurements on the statics and dynamics of polymers in flow has become possible because of the development of modern experimental techniques such as fluorescence microscopy [41, 42] and laser tweezers [43,44]. Molecular biology provides samples of model polymers like DNA [45,46] which are large enough to be observed directly when they are decorated with a fluorescent dye. These experimental techniques have since been applied to various forces [47] and flow fields [48–52] and to many other systems, *e.g.* DNA in concentrated solution [53,54]. Especially the investigation of polymers in extensional flow exhibited a great and unexpected variety of conformations [49,50,55].

This experimental progress with single polymers has stimulated theoretical investigations on the response of polymers to external fields [56–58]. Two approaches have been applied specifically to the case of a tethered polymer in a uniform flow as considered in this work: the blob model [59–61] and the dumbbell model [62].

The blob model has been widely used for the description of the static and dynamic properties of polymers pulled at the end [2,63,64]. From the theoretical point of view this model is very attractive because scaling laws for both global and local properties characterizing the extension and shape of the polymer can be derived analytically even in the presence of excluded volume and hydrodynamic interactions. Applied to a tethered polymer in flow [59–61], the blob model allowed the identification of distinct flow regimes corresponding to different shapes of the polymer. This shape is determined by the balance between thermal agitation and tension along the polymer. One can distinguish three regimes depending on the magnitude of the flow field. The local tension along the polymer increases from the free towards the fixed end of the chain. As long as the external forces are small the equilibrium structure of the polymers is only slightly distorted. This may be termed the near–equilibrium regime. For moderate forces the polymer still coils up at the free end due to thermal agitation, but towards the fixed end it becomes more and more unwound. This eventually leads to a polymer shape resembling a trumpet [59] (cf. Fig. 1) whence this is called the trumpet regime. For even larger values of the flow velocity there is a finite fraction of the polymer close to the fixed end which is already completely straightened whereas the free end is still coiled up. This has become known as the stem and flower regime [61]. The price for this insight, however, are the not immediately obvious assumptions and approximations used in the model. Their validity is well worth to be tested by polymer models like bead spring models (cf. Fig. 2) which resolve the many degrees of freedom of real polymers more faithfully.

On the other hand the more detailed bead spring model becomes very difficult to treat even numerically when excluded volume and hydrodynamic interactions are taken into account [33,65,66]. To facilitate calculations excluded volume effects are often neglected and an averaging approximation for the hydrodynamic interactions is introduced [30,67,68]. This procedure, however, is not com-

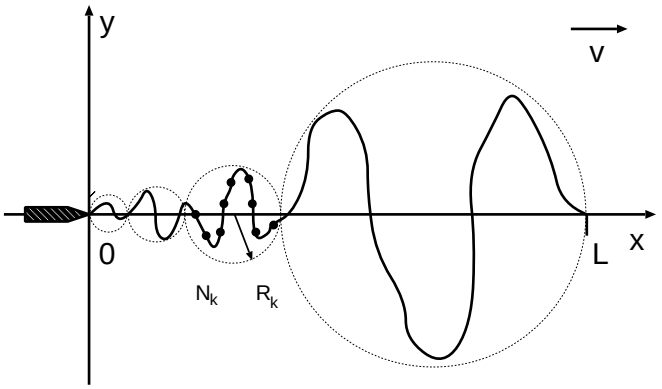

Fig. 1. Sketch of a polymer which is tethered at one end ($x = 0$) and subjected to a uniform flow of velocity v in the positive x–direction. For intermediate flow velocities it was suggested to describe the polymer by a string of blobs (large dotted circles) [59] with radius R_i containing N_i beads, cf. Fig. 2. It was predicted that in this regime the shape of the polymer resembles the form of a trumpet.

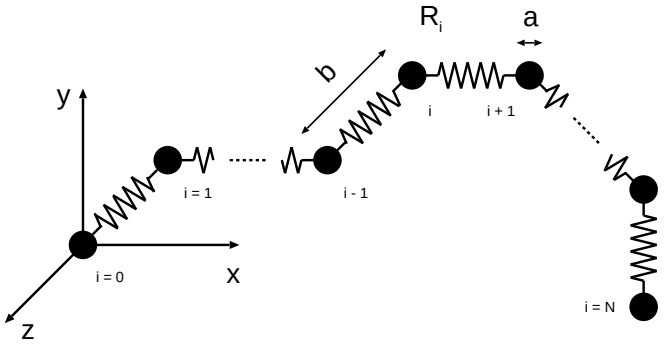

Fig. 2. Sketch of a bead spring model for a polymer [29–32] which is fixed at one end (bead index $i = 0$). The springs connecting the beads are either harmonic springs described by the quadratic potential in Eq. (28) or anharmonic springs with the nonlinear potential given in Eq. (71). The former gives a Gaussian distribution of the bond length $|\mathbf{Q}|$ while thermal equilibrium and the bonds are strongly stretched in the presence of flow. In the latter case the bond lengths remain almost unchanged unless the flow becomes very strong (cf. Sec.3). In appendix C we consider a chain where the springs are replaced by rigid rods of length b. This gives the freely jointed chain model.

pletely controlled. In fact, it removes the *nonlinearity* from the equations of motion and therefore necessarily leads to a Gaussian conformational distribution function [69]. An approach along these lines was also used to investigate a tethered polymer in uniform flow [62]. It was argued that the hydrodynamic interaction acts to keep the coil at the free end of the polymer tightly together so that it may be modelled as the one bead of a half–dumbbell model. The results from this half–dumbbell model were found to be in qualitative agreement with the experimental data.

It is difficult, however, to generalize these results to other conditions. According to its small number of degrees of freedom the dumbbell model cannot describe something like the transition between a coiled and a stretched state of the polymer [19,20]. It can also not describe a crossover between non–draining and free–draining polymer behavior as analyzed in this work. Finally it does not allow to calculate the perturbation of the imposed flow caused by the polymer. This latter step in our view, however, constitutes a second crucial part of the nonlinear interaction between the polymer molecules and the macroscopic flow of the solution next to the deformation of the polymer by the flow. An analytical description of this nonlinear interaction seems impossible at present.

The purpose of the present paper is to address some of the general questions raised above: the validity of the blob model, the relative importance of various interactions for the bead spring model and the number of beads which is necessary to faithfully describe the conformations of the polymer. As a specific case we consider these questions for a single polymer which is fixed at one end and subjected to a uniform flow in the x–direction. Here we concentrate on the deformation of the polymer at steady state. The explicit determination of the perturbation of the flow field and the relaxation dynamics of the polymer will be addressed elsewhere [70–72].

With respect to generality in the interactions only computer simulations of a long bead spring chain are promising in order to make progress on these issues. To avoid uncontrolled approximations in the hydrodynamic interactions two methods are applicable. In molecular dynamics calculations [73,74] the solvent is taken into account as a collection of individual particles and a canonical ensemble is realized by means of a thermostat. A problem arising in non-equilibrium systems is the realization of boundary conditions for which a standard scheme exists only for the case of simple shear flow [75,76]. Closer to the theory and as it turns out also favorably in terms of computer time are Brownian dynamics simulations [33] where the solvent degrees of freedom are integrated out of the equation of motion. This induces conformation dependent correlations in the stochastic forces which must be properly accounted for. We avoid averaging procedures [30,62, 67,68] and simulate the Brownian dynamics of the polymer including the full fluctuating hydrodynamics. For doing so the straight forward discretization scheme for the Langevin equation is modified to achieve large enough integration steps while still preserving the Boltzmann distribution at equilibrium [77,78]. In contrast to previous Brownian dynamics studies of polymers with fluctuating hydrodynamics [79–84] this allows simulations of reasonably long chains on present day high-speed supercomputers and a partial qualification of various model approaches becomes possible.

In section 2 the global and local properties of interest, *i.e.* measures for the extension of the polymer in the flow direction and perpendicular to it as well as the density of polymer segments, are defined and the quantities used within the blob models are related to those suitable for bead spring models. Results for these quantities are obtained for the Gaussian chain, *i.e.* a bead spring chain with harmonic springs and with no other interactions taken into

account. The methods we use are an analytical calculation based on the Gaussian conformational distribution function (cf. appendix B) and numerical simulations of the Langevin equation (cf. appendix E). The results for the Gaussian chain are compared to the predictions of a blob model making the same assumptions which is presented in appendix A. The scaling behavior of the blob model in this case agrees well with both the analytical calculation and the numerical simulations.

The unrestricted extensibility of polymer models with a Gaussian distribution of the bond lengths obviously conflicts with the fact that the chemical bonds ultimately impose a fixed contour length on the polymer. This constraint becomes an essential ingredient at larger flow velocities. In section 3 we investigate the global and local properties of a polymer in flow for the freely jointed chain and the FENE (**F**inite **E**xtensible **N**onlinear **E**lastic) chain. For both models several analytical results on the scaling behavior of the end–to–end distance and the segment density are derived in appendices C and D respectively. The scaling of the blob model is now approached only for very long chains and it holds only in a rather narrow range of velocities.

In section 4 we make the previous models more complete by taking into account the excluded volume effect for both the Gaussian chain and the FENE chain. It will be shown that the excluded volume effects vary along the deformed polymer. Finally in section 5 we add the effects of hydrodynamic interactions between the beads to both models by employing the Oseen tensor. A crossover between non–draining and free–draining polymer behavior will be demonstrated and the quantitative results of the simulations suggest that for real polymers one cannot expect the simple scaling behavior predicted by blob models with either non–draining or free–draining blobs.

We close this work with a discussion of the applicability of the different models and the relative importance of the various interactions. While the qualitative behavior of the polymer is described in sections 2–5 most of the details of the analytical calculations are given in appendices A for the blob model and appendices B through D for the Gaussian, freely jointed and FENE chains respectively. The main analytical scaling results are summarized in table 1. The details of the numerical simulations are described in appendix E and appendix F.

2 Tethered Gaussian chain in the free–draining limit

In this section we consider the simplest bead spring model (cf. Fig. 2) where the springs are harmonic and no other interactions between the beads are taken into account, the so–called Gaussian chain. For this model the polymer deformation can be calculated both by numerical simulation and by analytical methods which confirms the accuracy of the numerical scheme. However, analytical scaling laws for the extension of a tethered polymer in uniform flow as a function of the flow velocity and the number of polymer segments have first been derived for a blob model (cf. Fig. 1) for the *non*–draining limit [59], *i.e.* for the case with strong hydrodynamic interactions. In appendix A we therefore introduce a modified blob model for a polymer for the *free*–draining limit where the hydrodynamic interactions are neglected and we derive the scaling behavior of the extension $L(v)$ and the segment density along the flow direction $\rho(x)$ as well as the lateral extension $\Upsilon(x)$ of the polymer. These results are now compared with the analytical and numerical results for the more detailed Gaussian chain.

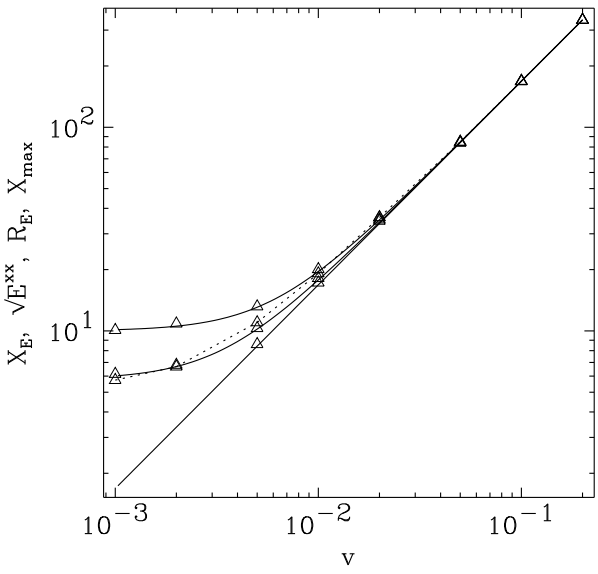

Fig. 3. Various measures for the chain extension as functions of the flow velocity v for a Gaussian chain with $N = 100$ beads: end–to–end distance R_E (upper curve), square root of the xx–component of the end–to–end tensor $\sqrt{E^{xx}}$ (middle solid curve), mean value of the x–coordinate of the end–to–end vector X_E (lower curve) and maximum x–coordinate among all beads X_{max} (dotted line as guide to the eye). The symbols are values obtained from numerical simulation; the analytical results are due to Eqs. (1 –3).

For the bead spring model there are several possible measures of the in–flow extension of the polymer [32] as shown in Fig. 3: the end–to–end distance R_E (upper solid curve), the square root of the end–to–end tensor $\sqrt{\mathsf{E}^{xx}}$ (middle solid curve), the mean x–component of the end–to–end vector X_E (lower solid curve) and the mean value of the maximum x-coordinate among all beads $X_{max} = \langle \max_i (R_i^x - R_0^x) \rangle$ (dotted line). X_{max} cannot be calculated analytically (the dotted line in Fig. 3 is only a guide to the eye) but the other quantities are easily obtained analytically from the conformational distribution function as detailed in appendix B.2. The corresponding solid lines in

Fig. 3 are calculated according to the relations

$$R_E = \sqrt{\langle |\mathbf{R}_N - \mathbf{R}_0|^2 \rangle} = \left(b^2 N + \left(\frac{b^2 \zeta v}{3 k_\mathrm{B} T} \, \frac{N\,(N+1)}{2} \right)^2 \right)^{1/2} , \quad (1)$$

$$\sqrt{\mathsf{E}^{xx}} = \sqrt{\langle (R_N^x - R_0^x)^2 \rangle} = \left(\frac{b^2}{3} N + \left(\frac{b^2 \zeta v}{3 k_\mathrm{B} T} \, \frac{N\,(N+1)}{2} \right)^2 \right)^{1/2} , \quad (2)$$

$$X_E = \langle R_N^x - R_0^x \rangle = \frac{b^2 \zeta v}{3 k_\mathrm{B} T} \, \frac{N\,(N+1)}{2} . \quad (3)$$

Here b is the root mean square bond length at equilibrium, N is the number of beads used in the model, ζ is the single bead friction coefficient, and v is the velocity of the flow in the x–direction. ζ is related to the solvent viscosity η and the effective hydrodynamic bead radius a by Stokes law $\zeta = 6\pi\eta a$. The values obtained from numerical simulation for all four quantities, R_E, $\sqrt{\mathsf{E}^{xx}}$, X_E and X_{max}, are given by the symbols in Fig. 3. They are found in perfect agreement with the available analytical results.

When the polymer is sufficiently elongated, that is at large enough flow velocities, *e.g.* $v \gtrsim 0.05$ for $N = 100$ as used in Fig. 3, then all quantities exhibit the same scaling. For small values of the flow velocity X_E tends to zero while the other quantities remain finite. At $v = 0$ the size of the polymer coil is determined solely by thermal fluctuations. Therefore we may say that X_E measures only the elongation caused by the external flow acting against the entropic elasticity of the polymer while the other quantities include some contribution that is due to thermal fluctuations directly. At some flow velocity the latter contribution becomes negligible and all quantities agree with each other.

For vanishing flow velocity, $v = 0$, Eq. (1) reduces to the well-known Flory law for the end–to–end distance as a function of the number of beads N [2,31,32,85]. The two experimentally accessible lengths $R_E = N^{1/2} b$ and Nb then fix the model parameters N and b. These are interpreted as the number and size of statistically independent parts of the chain, the so-called Kuhn segments [86].

If our main focus is on the regime at larger flow velocities where the drag forces exerted by the external flow dominate the thermal forces, there is more freedom in the choice of the model parameters. In this case only the contour length of the polymer is relevant which fixes only the product Nb. Furthermore in the free–draining case considered here each bead experiences a drag force ζv, *i.e.* the total drag force experienced by the whole chain is $N\zeta v$. If we take b and ζ as units for length and force chains with a different number of beads N may be compared by looking at the fractional extension $X_E/(Nb)$ as a function of the total drag $N\zeta v$. Rewriting Eq. (3) as

$$\frac{X_E}{Nb} = \frac{b}{6 k_\mathrm{B} T} \zeta v (N+1) \quad (4)$$

one finds that the functional relation between the two quantities is indeed independent of N provided N is large compared to 1. If we use R_E in place of X_E the curves for different N will not collapse for small values of v because in this case the velocity independent contribution in Eq. (1) cannot be neglected. This may also be used as an indicator that the direct contribution of the thermal fluctuations to the polymer extension is important.

The polymer extension L as calculated within the free–draining blob model in appendix A is

$$L \propto \left(\frac{\eta a}{k_\mathrm{B} T} \right) v (Nb)^2 . \quad (5)$$

Both the linear scaling with the flow velocity v and the quadratic scaling with the number of beads N agree with that for the various quantities in Eqs. (1)–(3) for large enough values of v, where the velocity independent contributions can be neglected. Hence a tethered polymer may be described as a string of blobs as indicated in Fig. 1 if the chain is sufficiently elongated. For small elongation or equivalently for small flow velocity the blob picture is no longer valid as also discussed in appendix A. A quantitative estimate of the range of validity of the blob model is furnished by comparing the scaling of the length of a string of blobs $L \propto v$ given by Eq. (5) with the different measures of chain elongation for the more detailed bead spring model shown in Fig. 3. The mean x–component of the end–to–end vector X_E scales linearly with v and thus has the same scaling as the chain extension L in the blob model while the other quantities deviate from this scaling behavior at small flow velocities. Based on the interpretation of X_E given before, this suggests that the blob model describes only that part of the polymer extension which is due to the action of the flow. Since the other quantities like the end–to–end distance R_E also contain the direct contribution of the thermal fluctuations, a vanishing difference $R_E - X_E$ might be a reasonable measure for the range of validity of the blob model. This is also confirmed by looking at the exponent μ for the segment density at different flow velocities (see below).

Eqs. (1)–(3) indicate that the whole contour of a tethered Gaussian chain is considerably stretched with increasing values of the flow velocity because the end–to–end distance can grow without bounds, *i.e.* for $N = 100$, R_E exceeds the contour length at equilibrium Nb for $v \gtrsim 0.05$. This feature can be traced down to a stretching of the individual springs, the mean square length $\langle |\mathbf{Q}_k|^2 \rangle$ of which is given by Eq. (38). Since the blob model uses a constant value $\langle |\mathbf{Q}_k|^2 \rangle = b^2$ in each blob it is not obvious why the blob model predicts the correct scaling behavior for the Gaussian chain. This question will be discussed in more detail later on.

Local information about the polymer shape is provided by the density of polymer segments along the flow direction $\rho(x)$. The blob model yields an analytical expression for the density $\rho(x_0 - x)$ measured from the free chain end x_0 which shows an inverse power law behavior

$$\rho(x_0 - x) \propto \frac{1}{b} \left(\frac{k_\mathrm{B} T}{\eta a} \right) v^{-1/2} (x_0 - x)^{-1/2} , \quad (6)$$

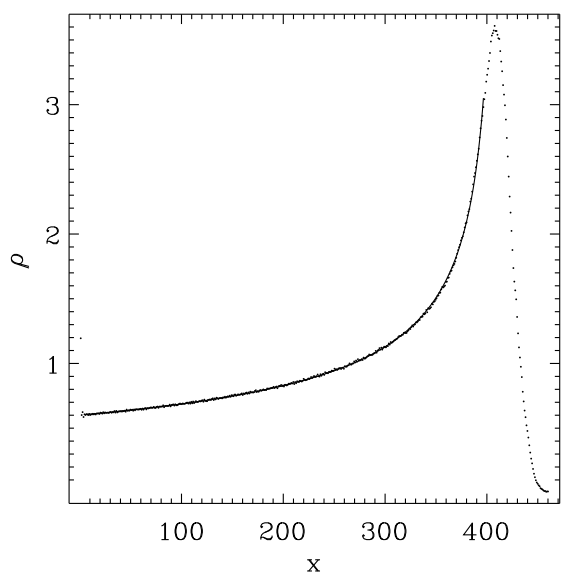

Fig. 4. Distribution $\rho(x)$ of polymer segments along the flow (x–) direction as obtained from simulation of a chain with $N = 500$ beads connected by harmonic springs at a flow velocity of $v = 0.01$. The solid line is a fit according to the formula $\rho(x) \propto \alpha(x_0 - x)^{-\mu}$ with the fitted values $\mu = 0.48$, $x_0 = 409.6$ and $\alpha = 10.86$. The x-range for the fit (here $x \in [5.6, 396.6]$) has been chosen such as to maximize the number of data points in agreement with the fit. Close to the tetherpoint at $x = 0$ the segment density may be smaller than 1 because the segments of the Gaussian chain are stretched beyond their equilibrium length b.

as shown in in appendix A. Here again b is the Kuhn length and a the hydrodynamic bead radius. This expression diverges at the position x_0 of the free end of the polymer.

In numerical simulations of a chain with $N = 500$ beads connected by harmonic springs we obtain a segment density as shown in Fig. 4 at medium values of the flow velocity ($v = 0.01$). Here $\rho(x)$ is normalized to give the number of beads N. The solid curve is a fit to the power law $\rho \propto \alpha(x_0 - x)^{-\mu}$ where the fitted exponent $\mu = 0.48$ is rather close to the exponent $1/2$ in Eq. (6), the analytical expression obtained from the blob model. For the additional fit parameters we find values of $x_0 = 409.6$ and $\alpha = 10.86$. Since x_0 is only slightly beyond the location of the maximum of $\rho(x)$ it is tempting to identify x_0 with the position of the free chain end in the blob model.

The velocity $v = 0.01$ for which the data in Fig. 4 have been obtained is just at the onset of the validity range of the blob model (trumpet regime) as determined from the difference $R_E - X_E$ for $N = 500$. For smaller flow velocities we find a decreasing exponent μ thus confirming the agreement of R_E and X_E as a quantitative measure for the validity range of the trumpet regime.

The segment density $\rho(\mathbf{r})$ as derived from the conformational distribution function in appendix B.4 is given by

$$\rho(\mathbf{r}) = \left\langle \sum_{k=0}^{N} \delta(\,\mathbf{r} - \mathbf{R}_k\,) \right\rangle \tag{7}$$
$$= \delta(\,\mathbf{r} - \mathbf{R}_0\,) + \sum_{k=1}^{N} \left(\frac{3}{2\pi k b^2}\right)^{\frac{3}{2}} \exp\!\left(-\frac{3}{2kb^2}\;(\mathbf{r} - \langle \mathbf{R}_k \rangle)^2\right).$$

This is a sum of Gaussian distributions centered about the mean position of the k–th bead $\langle \mathbf{R}_k \rangle$. Evaluating Eq. (7) numerically for a large number of beads ($N = 5000$) the functional dependence of $\rho(x)$, which is obtained from $\rho(\mathbf{r})$ by integrating over y and z, is seen to follow nearly exactly the power law $\rho \propto (x_0 - x)^{-1/2}$ when a small fraction of beads close to the free end is discarded.

In appendix B.5 we introduce an alternative measure for the local density of polymer segments along the x–axis by the inverse mean distance in the x–direction between neighboring beads. This so–called quasi–segment density takes the form

$$\rho'(x_0 - x) = \frac{1}{b}\sqrt{\frac{3k_{\mathrm{B}}T}{2\,\zeta\, v\,(x_0 - x)}}\,, \tag{8}$$

which again shows the scaling behavior $\rho \propto (x_0 - x)^{-1/2}$. Note that the quasi–segment density has the same scaling as the segment density in the blob model for *any* number of beads and over the *whole* range of x–positions. In contrast the true segment density, obtained either from simulation or from the conformational distribution function, shows the scaling predicted by the blob model only for long chains and away from the free chain end. The quasi–segment density which is based only on the *mean* bead–positions can be considered as a mean–field type approximation to the true segment density. The true segment density also accounts for the *fluctuations* of the beads around these mean positions which is obvious from the result in Eq. (7) which is a sum of Gaussian distributions each located at the mean position of one of the beads. This is the reason for the deviations between the true and the quasi–segment density for short chains and at the free end. The complete agreement between the quasi–segment density and the blob model again suggests to view the latter as a mean–field type theory.

Another quantity that has been used to characterize the polymer shape within the blob model is the polymer extension perpendicular to the flow direction $\Upsilon(x)$. One obtains for the blob model in the free–draining limit, cf. appendix A, the formula

$$\Upsilon(x) \propto b\left(\frac{k_{\mathrm{B}}T}{\eta a}\right)^{1/2} v^{-1/2}(x_0 - x)^{-1/2}\,, \tag{9}$$

which describes a trumpet shape of the envelope of the polymer coil. This quantity has no direct correspondence within the bead spring model. We attempt to relate $\Upsilon(x)$ to the 2–dimensional segment density $\rho(x, y)$ in the following way: For each value of the x–coordinate we distribute

the total weight $\rho(x)$ in the y-direction according to a distribution $\mathcal{P}(y(x))$. A particular choice for $\mathcal{P}(y(x))$ could be a Gaussian with variance $\Upsilon(x)$. Then we can calculate the yy-component of the gyration tensor which is the second moment of the segment density [31] as

$$G^{yy} = \int dx\, \rho(x) \int dy\, y^2\, \mathcal{P}(y(x)) = \int dx\, \rho(x)\, \Upsilon(x)\,. \quad (10)$$

For the second equality we used the fact that the y-integral is precisely the variance of $\mathcal{P}(y(x))$ which is $\Upsilon(x)$ by our construction. If we insert the relations for $\Upsilon(x)$ and $\rho(x)$ from Eq. (9) and Eq. (6) we can put the velocity dependent prefactors in front of the integral and thus obtain a prediction of the scaling behavior of the yy-component of the gyration tensor with the flow velocity v, namely $G^{yy} \propto v^{-1}$. Note that this power law does not depend on the precise form of $\mathcal{P}$; the only property of $\mathcal{P}$ that really matters is its second moment.

The power law for G^{yy} is readily compared to the corresponding result for a bead spring model. Here the gyration tensor is defined as

$$\mathsf{G} = \frac{1}{2N^2} \left\langle \sum_{i=1}^{N} \sum_{j=1}^{N} (\mathbf{R_i} - \mathbf{R_j})(\mathbf{R_i} - \mathbf{R_j})^T \right\rangle . \quad (11)$$

Due to symmetry we can use the transverse component of the gyration tensor

$$G^{\perp} = \frac{1}{2}(G^{yy} + G^{zz}) \quad (12)$$

in place of G^{yy} which gives a better statistics when evaluated from numerical data.

The result for the Gaussian chain derived in appendix B.3 is

$$G^{\perp} = \frac{1}{2N^2} \left(\frac{1}{3} N^3 + \frac{2}{3} N \right) \frac{b^2}{3}\,, \quad (13)$$

which is independent of the flow velocity. Therefore we conclude that the blob model is not able to make predictions about the transverse extension of a Gaussian chain in flow.

3 Chains of finite extensibility

The tethered Gaussian chain discussed in the previous section may be stretched by a flow unrealistically strong beyond its equilibrium contour length. For this reason we investigate in this section more realistic polymer models where the contour length is fixed or only slightly stretched by a flow.

A suitable model for numerical simulations is a bead spring chain with a nonlinear (FENE) spring potential as given by Eq. (69) (see *e.g.* [87–89]). We calculate the unwinding of a tethered FENE chain in a uniform flow field both numerically and semi–analytically in a similar manner as in the previous section for the Gaussian chain.

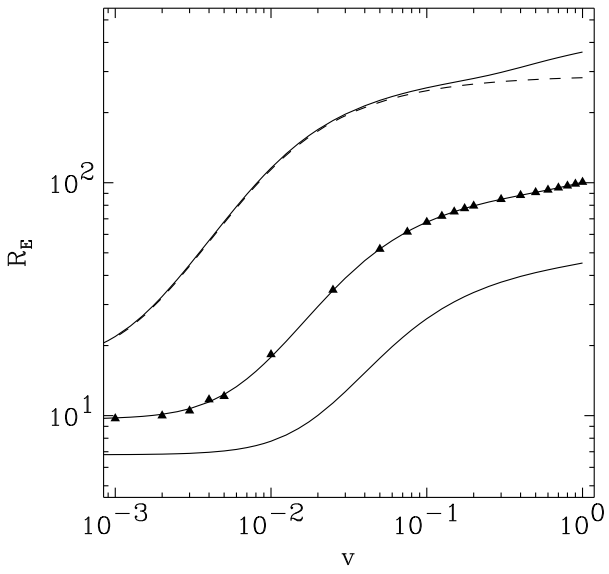

Fig. 5. End–to–end distance R_E for a tethered FENE chain in the free–draining limit as a function of the flow velocity v for different chain lengths $N = 50$ (bottom), $= 100$ (middle), $N = 300$ (top). The symbols are data obtained from numerical simulation while the solid lines are obtained from evaluation of the integrals in Eq. (77). The dashed line is the result for the freely jointed chain for $N = 300$ as given by Eq. (64).

The semi–analytical part, *i.e.* the derivation of the formula for the end–to–end distance, is described in detail in appendix D. We then compare the results for the FENE model to those for a freely jointed chain which prohibits any stretching of the bonds at all. This model can also be treated analytically to some extent as described in appendix C.

The flow velocity dependence of the end–to–end distance R_E of a FENE chain is shown in Fig. 5 for different chain lengths Nb where $b = 0.961$ (cf. appendix D). The solid lines are obtained by evaluating the integrals in Eq. (77) and the symbols are the results of numerical simulations of a FENE chain with $N = 100$ beads.

Three different regimes can be recognized in Fig. 5. For very large velocities the end–to–end distance is still growing slowly with some power law $R_E \propto v^{0.3}$. This nonzero but small exponent indicates a residual stretching of FENE chains in very strong flow fields. For comparison the end–to–end distance of a freely jointed chain with $N = 300$ beads is calculated according to Eq. (64) and shown by the dashed line in Fig. 5. Beyond $v \simeq 0.1$ the freely jointed chain is almost completely uncoiled as indicated by the plateau of the dashed curve. Comparing the upper solid line in Fig. 5 with this dashed line gives an estimate of the stretchability of the FENE chain which is only noteworthy for $v \gtrsim 0.1$ at $N = 300$. Hence for smaller flow velocities there is no significant difference between the FENE and the freely jointed chain. An examination

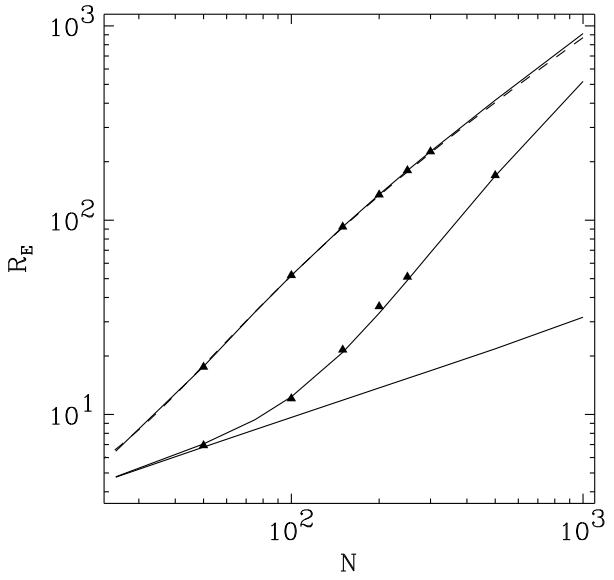

Fig. 6. End–to–end distance R_E for a tethered FENE chain in the free–draining limit as a function of the number of beads N for different flow velocities $v = 0.0005$ (bottom), $v = 0.005$ (middle), $v = 0.05$ (top). The symbols are data obtained from numerical simulation while the solid lines are obtained from evaluation of the integrals in Eq. (77). The dashed line is the result for a freely jointed chain for $v = 0.05$ as given by Eq. (64).

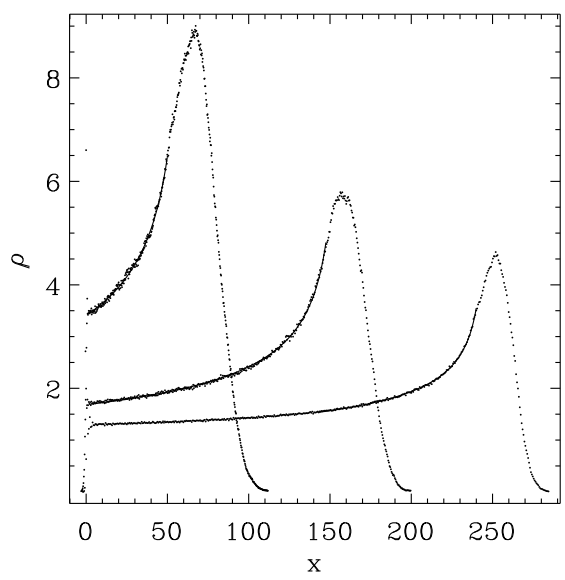

Fig. 7. Distribution $\rho(x)$ of polymer segments along the flow (x–) direction as obtained from simulation of a chain with $N = 500$ beads connected by FENE springs and for three different flow velocities $v = 0.002$ (left), $v = 0.005$ (middle) and $v = 0.01$ (right). The solid lines are a fit of the curves with the formula $\rho(x) \propto \alpha(x_0 - x)^{-\mu}$. The values of the fit-parameters are $\mu = 0.37$, $x_0 = 61.09$, $\alpha = 16.05$ for $v = 0.002$, $\mu = 0.35$, $x_0 = 155.2$, $\alpha = 9.87$ for $v = 0.005$ and $\mu = 0.28$, $x_0 = 245.4$, $\alpha = 5.76$ for $v = 0.01$. The x-ranges for the fit ([1.6,49.9],[1.6,147.9] and [142.5,140.5]) have been chosen such as to maximize the number of data points in agreement with the fit. In contrast to the Gaussian chain (cf. Fig. 4) the segment density is now always greater than one.

of the distribution of bond lengths at different flow velocities shows that the onset of the residual stretchability is roughly inversely proportional to N. In an intermediate velocity regime the end–to–end distance for the FENE chain behaves as $R_E \propto v^{0.84}$ for $N = 300$. The exponent increases with N until it is expected to reach a fixed value of 1 for very long chains which is the value obtained for the freely jointed chain with $N = 5000$ in a tiny range of flow velocities (cf. Fig. 8). Finally for very small velocities the polymer coil is almost undisturbed and the end–to–end distance is close to its value in thermal equilibrium.

The N–dependence of the end–to–end distance is shown in Fig. 6 for different flow velocities. At small velocities R_E increases with $N^{1/2}$ which is the same as the N–dependence at thermal equilibrium. Again the influence of the residual extensibility of the FENE chain can be assessed by comparing in Fig. 6 the solid line for $v = 0.05$ with the dashed line, where the latter belongs to the end–to–end distance for the freely jointed chain given by Eq. (64). Here even for the largest number of beads the deviations are still very small indicating that at such velocities the FENE chain is stretched by a tiny amount only.

The segment density $\rho(x)$ for a FENE chain with $N = 500$ beads is shown in Fig. 7 and for three different flow velocities $v = 0.002$, $v = 0.005$ and $v = 0.01$. The shape of $\rho(x)$ is qualitatively similar to that for a Gaussian chain, (cf. Fig. 4), and this trumpet shaped distribution can again be fitted by an inverse power law $\rho \propto \alpha(x_0 - x)^{-\mu}$. The precise values of all fit parameters are given in the caption of Fig. 7. For the exponent μ one obtains values between $\mu = 0.37$ and $\mu = 0.28$. These exponents are significantly smaller than the value $\mu = 0.5$ obtained for the Gaussian chain which is a consequence of the limited stretchability of the chain segments.

To investigate the validity of the scaling predictions of the blob model we show in Fig. 8 the x-coordinate of the end–to–end vector X_E and the end–to–end distance R_E as functions of the flow velocity for freely jointed chains with $N = 500$ and $N = 5000$ beads. This compares to Fig. 3 for the Gaussian chain. Again the validity of the blob model may be expected only in the range where the curves for X_E and R_E in Fig. 8 coincide. In contrast to the Gaussian chain, here the scaling of the blob model, $L \propto v$, applies only in some small transition regime, roughly between the two velocities $v_{c1} \sim 6 \times 10^{-5}$ and $v_{c2} \sim 4 \times 10^{-4}$ for $N = 5000$. For $N = 500$ no scaling regime is visible in Fig. 8. That there is now also an upper limit for the scaling regime is obvious since the finite extensibility requires the extension to have a plateau at large velocities. The N–dependence of the size of the validity range of the trumpet

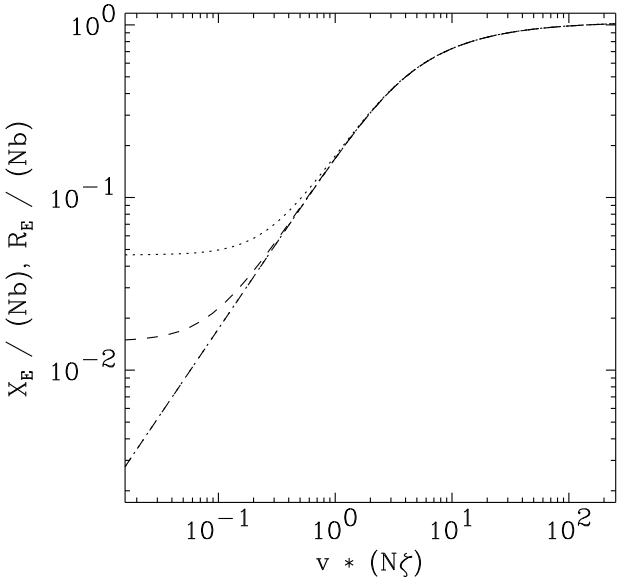

Fig. 8. Flow velocity dependence of the end–to–end distance R_E according to Eq. (64) (upper curves) and the x–coordinate of the end–to–end vector X_E according to Eq. (62) (lower curves) for freely jointed chains with $N = 500$ (dotted curves) and $N = 5000$ (dashed curves) beads. The axes are scaled such that curves with different N collapse for sufficiently large v as explained in the previous section. The agreement between the curves for X_E is so perfect that they can hardly be distinguished.

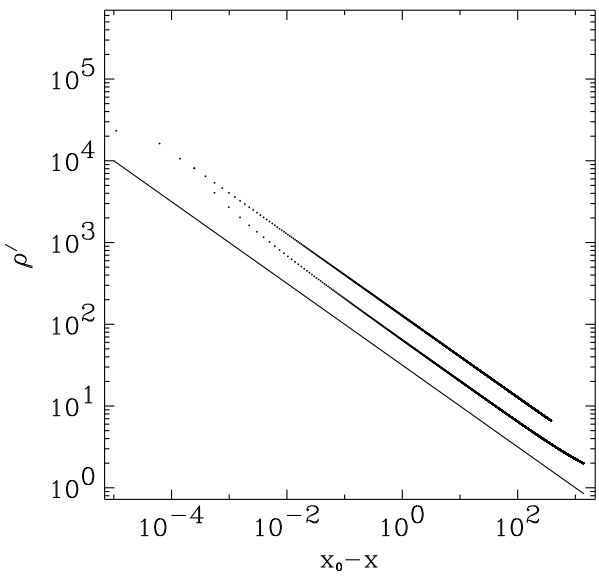

Fig. 9. Quasi–segment density $\rho'(x)$ according to Eqs. (66)–(67) for a freely jointed chain with $N = 5000$ beads and for flow velocities $v = 1 \times 10^{-4}$ (top) and $v = 4 \times 10^{-4}$ (middle). The lower solid line gives the blob scaling $\rho' \propto (x_0 - x)^{-1/2}$. The ordinate here is $x_0 - x$ instead of x which is different in Fig. 4 and Fig. 7.

regime is given in Eq. (26) for the free–draining and in Eq. (27) for the non–draining blob model (cf. Ref. [61]). This N–dependence is rather weak whence it is already clear form these formulae that *very* long chains are needed to exhibit a clear scaling regime. According to the estimate given above $N = 5000$ is barely sufficient since it gives only a tiny scaling regime. Therefore, for non-stretchable chains of only up to $N \simeq 3000$ Kuhn segments like the DNA used in experiments [39,49,62] one can hardly expect a trumpet regime for the polymer deformation even in the free–draining limit. As we show in the next sections excluded volume and hydrodynamic interactions require even longer chains to reach a scaling regime.

Beyond the validity range of the trumpet regime a so–called stem and flower regime was suggested [61]. In this regime the polymer is divided into two parts. The stem is the completely straightened part close to the fixed end where $\rho(x) = 1$ and the flower is the part close to the free end where the usual trumpet scaling holds, *i.e.* $\rho(x) \propto x^{-1/2}$.

This scaling of the segment density is an additional, local measure for the validity of the blob model. To check the behavior in the long–chain limit for the freely jointed chain we have to rely on the quasi–segment density $\rho'(x)$ (cf. appendix B and C) because there is no simple analytic result for the true segment density. The quasi–segment density has been shown to give the same scaling as the true segment density for the Gaussian chain in the previous section. We emphasize, however, that both quantities are not equivalent.

For a freely jointed chain with $N = 5000$ we indeed find a power law behavior $\rho' \propto (x_0 - x)^{-1/2}$ as for the blob model in a small range of flow velocities around $v = 1 \times 10^{-4}$ as shown by the upper curve in Fig. 9. For both smaller and larger flow velocities there is a deviation from the scaling close to the free end which may be attributed to a break-down of the mean–field type approximation used in the definition of ρ' (cf. section 2). For larger flow velocity (middle curve in Fig. 9) there is an additional deviation close to the fixed end which indicates the development of a stem.

The estimate just made for the range of flow velocities where the trumpet regime may be observed agrees with that obtained from the analysis of the global chain extension in Fig. 8. It also seems to indicate that the densities for FENE chains with $N = 500$ shown in Fig. 7 correspond already to the stem and flower regime. However, the fitted scaling exponents differ strongly from the value of $1/2$ even when the fit range was restricted to some portion of the chain near the free end. In order to understand this we note that the appearance of the blob scaling for $\rho'(x)$ depends crucially on a precise knowledge of the location of the free chain end. This allows to make a logarithmic plot of $\rho'(x)$ from which a local (x–dependent) exponent can be read off and to see for which x–positions it has a value of $1/2$. For the true segment density $\rho(x)$, however,

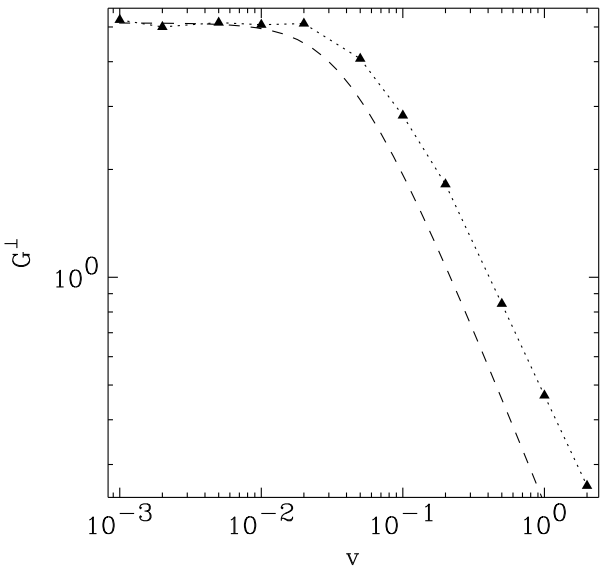

Fig. 10. Flow velocity (v–) dependence of the transverse component of the gyration tensor $G^{\perp}$ for a FENE chain (triangles) and a freely jointed chain (dashed line) with $N = 100$ beads. The data for the FENE chain are calculated from numerical simulations; the curve for the freely jointed chain is obtained by evaluating the sum in Eq. (65).

the location of the free chain end is not even well-defined and one has to use a fit procedure with a prescribed range of x–positions to obtain a single global exponent. Fitting the data for the quasi–segment density in a manner similar to those for the true segment density in Fig. 7 with an additional fit parameter x_0, one finds that the largest portion of the chain (located close to the fixed end and thus heavily squeezed in Fig. 9) is well fitted with exponents similar to those obtained for the true segment density for all flow velocities. The difference in these fitted values is already negligible for chains with $N = 500$ beads indicating that the asymptotic regime is reached even for $N = 500$. We conclude that the segment density is maybe not a good observable to discriminate between the trumpet and the stem and flower regime because fluctuations tend to smear out the different scaling $\rho \propto x^{\mu}$ in the stem ($\mu = 0$) and in the flower ($\mu = 1/2$). In addition at small flow velocities the exponent μ is reduced gradually as the blob model ceases to be valid which was observed already for the Gaussian chain.

In Fig. 10 we compare the transverse component of the gyration tensor $G^{\perp}$ as defined in Eq. (12) for a FENE and a freely jointed chain with $N = 100$ beads. At small flow velocities the values of $G^{\perp}$ for both models agree with each other and also with the value for a Gaussian chain which is $G^{\perp} = 5.13$ for $N = 100$ and $b = 0.961$ (cf. Eq. (44)). At large flow velocities $G^{\perp}$ obeys a power law for both models. The exponent, however, is different in both cases. For the FENE chain $G^{\perp} \propto v^{-0.8}$ while for the freely jointed chain $G^{\perp} \propto v^{-0.95}$. The transverse extension seems to be far more sensitive to the residual stretchability of the FENE springs than the elongation of the chain in the flow direction. Appreciable differences between the FENE and the freely jointed chain are already present at a flow velocity of $v = 0.02$ for $G^{\perp}$ while the values of R_E for both models agree with each other up to $v = 0.3$ for $N = 100$.

A power law behavior for the transverse extension is also predicted by the blob model when G^{yy} is calculated from $\Upsilon(x)$ as discussed in the previous section (cf. Eq. (10)). The predicted value of -1 for the exponent is in good agreement with the value obtained for the freely jointed chain. However, the range where the scaling regime for $G^{\perp}$ appears is at larger flow velocities than the range of the scaling regime for R_E. Extrapolating the estimate drawn from Fig. 8 the scaling range for R_E *extends* only up to $v0.02$ for $N = 100$ while the scaling range for $G^{\perp}$ in Fig. 10 *begins* only at $v \simeq 0.1$. Therefore some doubt remains as to whether the blob model faithfully describes the transverse extension of a freely jointed chain. Anticipating some results from section 5 we find that for the bead spring model the scaling exponent for $G^{\perp}$ does not depend on whether hydrodynamic interactions are included in the model or not. The non–draining blob model, however, predicts $G^{yy} \propto v^{-1/\nu}$ which is different from the prediction $G^{yy} \propto v^{-1}$ for the free–draining case discussed above and in section 2.

4 Excluded volume effects

For strongly elongated polymers the excluded volume interaction **(EVI)** can be neglected and the assumptions made in the previous two sections are justified. EVI only becomes important for smaller values of the flow velocity, where the equilibrium conformation is only moderately distorted. Only in this regime scaling exponents can be expected which are typical for EVI. Within the blob model the effects of EVI are easily covered by choosing the exponent of the Flory scaling $\nu = 3/5$ instead of $\nu = 1/2$ in Eq. (15). For the bead spring model with EVI one has to rely on numerical simulation since semi–analytical methods as used in the previous two sections are not tractable.

In Fig. 11 the end–to–end distance R_E is plotted for chains with $N = 100$ beads connected either by harmonic springs or by FENE springs and both with and without EVI. For large flow velocities corresponding to strong deformations the EVI becomes less important and therefore the curves with and without EVI approach each other for the Gaussian as well as for the FENE chains. With decreasing flow velocity in contrast, the differences between chains with and without EVI increase and for vanishing flow velocity R_E approaches its equilibrium value which is larger with EVI [2,31,32]. In thermal equilibrium, *i.e.* at $v = 0$, the end–to–end distance is basically the same for both the Gaussian and the FENE chains.

For the Gaussian chain at intermediate flow velocities, and therefore at medium deformations, the extension of

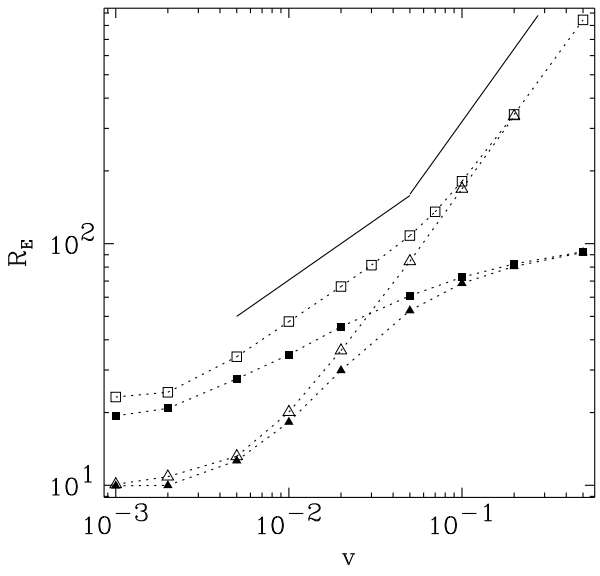

Fig. 11. End–to–end distance R_E as a function of the flow velocity for Gaussian (open symbols) and FENE (solid symbols) chains with $N = 100$ beads. The squares give data with excluded volume interactions (EVI) taken into account, the triangles give data without excluded volume interactions. The solid lines with slopes 0.5 and 1.0 correspond to the scaling exponents extracted from the data for the Gaussian chain. For vanishing flow velocity (thermal equilibrium) the curves for the FENE and Gaussian chains approach each other as expected in both cases with and without EVI. The small differences in the case with EVI are due to the slightly different effective bond lengths (cf. appendix E): for the Gaussian chain we have $b = 1.0$ without EVI and $b = 1.37$ with EVI while for the FENE chain $b = 0.961$ both with and without EVI.

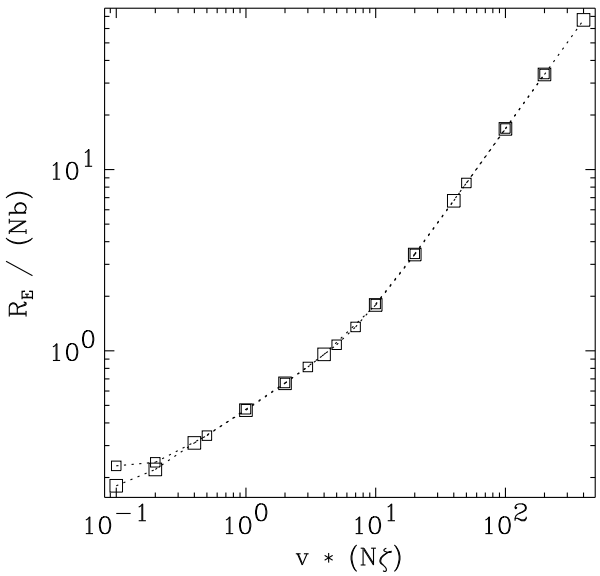

Fig. 12. Normalized end–to–end distance $R_E/(Nb)$ for chains of different lengths Nb (small and large squares) as a function of the total drag force exerted on the chain. The model assumes harmonic springs and only the excluded volume interaction (EVI) is taken into account. The numbers of beads for the two cases were $N = 100$ and $N = 200$ while the effective bond length is $b = 1.37$ for the Gaussian chain with EVI as explained in appendix E. The total drag force is just $vN\zeta$ in the free–draining case considered here.

polymer chains with and without EVI has a different scaling with velocity. In the uppermost curve of Fig. 11 we observe a scaling for the end–to–end distance $R_E \propto v^{0.5}$. Increasing N to 200 does not change the exponent by any significant amount (cf. Fig. 12). Between $v = 0.05$ and $v = 0.1$ there is a crossover to the scaling $R_E \propto v$ which is the same power law as for a Gaussian chain without EVI considered in section 2. This crossover takes place at a flow velocity where the extension of the polymer approximately equals the contour length of the polymer in thermal equilibrium. The scaling in the intermediate range, $R_E \propto v^{0.5}$, must be compared with the scaling of the extension $L \propto v^{2/3}$ for a blob model with EVI in the free–draining limit as described in appendix A.

In Fig. 12 the $R_E(v)$ curves are compared for two chain lengths $N = 100$ and 200. As explained in section 2 the curves for different N are expected to collapse for sufficiently large v when the fractional extension $R_E/(Nb)$ is plotted versus the total drag force which is $N\zeta v$ since the chain is free–draining. The two curves in Fig. 12 indeed agree so perfectly that we consider it as significant even though the values of N we considered differ only by a factor of two.

For the exponent μ for the segment density $\rho \propto (x_0 - x)^{-\mu}$ as calculated from numerical simulations of a chain with harmonic springs and EVI we find values between 0.3 and 0.4 in the intermediate velocity range $v = 0.005 \ldots 0.05$. For the blob model with $\nu = 3/5$ one has $\mu = 2/5$ as described in appendix A. These values are quite different from $\mu = 0.5$ for the case without EVI (cf. section 2).

In contrast to the good agreement between the scaling laws for the blob model and the Gaussian chain without EVI found in section 2, the agreement is less perfect when EVI is included. A possible explanation is simply that our chains even with $N = 200$ are too short. However, there is a more serious inherent problem in the blob model with EVI. Blob models can only be applied beyond some critical velocity where the polymer is sufficiently deformed. Then the deformation is stronger close to the tether point than near the free end. Therefore the EVI is less important near the tether–point than near the free end, *i.e.* the EVI becomes effectively x–dependent. But in the blob model one and the same exponent ν characteristic for EVI is assumed in each blob independent of its location close to the free or close to the tethered chain end. Therefore one can hardly expect a precise agreement between the scaling predicted by blob models with EVI and bead spring chains with EVI. Whether the position dependence of the

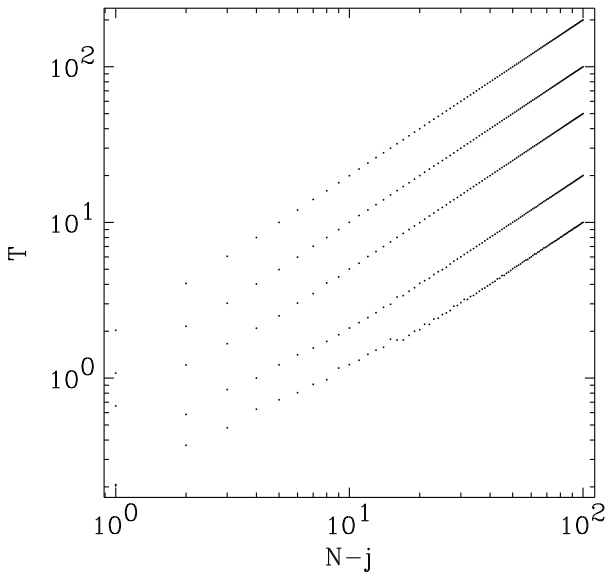

Fig. 13. Tension along the chain as a function of the bond index $N-j$ counted from the free chain end for different values of the flow velocity $v = 0.1$, 0.2, 0.5, 1.0, 2.0 from bottom to top. The data have been obtained from numerical simulations of a chain with $N = 100$ beads connected by harmonic springs including the excluded volume interaction (EVI). For the largest velocity (uppermost curve) the tension is proportional to the bond index indicating that EVI is unimportant for the uncoiled polymer.

EVI becomes unimportant in some velocity range for very long chains is unclear and it is not possible to attack this question seriously with present day computers.

The inhomogeneity of the EVI along the chain can clearly be seen directly from the tension within different parts of the chain. In Fig. 13 the tension T_{N-j} is shown as a function of the bond index $N-j$ for several values of the flow velocity v. Without EVI the tension increases linearly from the free ($N-j=1$) towards the fixed ($N-j=N$) chain end because the same drag force is exerted on each bead. This is the case for the largest velocity (uppermost curve) in Fig. 13 indicating that as expected EVI doesn't play a role anymore at large v when the polymer is strongly elongated. At smaller flow velocities the EVI, which couples even beads that are far apart along the chain, provides a mechanism to redistribute tension within the chain. As a consequence the tension within the first spring at the free chain end is larger than ζv which can clearly be seen in Fig. 13. Furthermore the slope of the T_{N-j} curve is reduced below 1 near the free chain end, *e.g.* to ~ 0.77 for $v = 0.1$. Near the fixed chain end where the chain is stretched stronger the EVI is already unimportant and T_{N-j} increases linearly with $N-j$. Altogether the tension within the very last spring near the fixed chain end again contains the total tension $N\zeta v$ expected in the free–draining limit. In the coiled portion of the chain where EVI is important contains only $10-20$ % of all beads at the smallest value of v shown in Fig. 13 but its trend to grow with decreasing flow velocity can be expected to continue also at smaller v where the statistical errors in the data become large.

For the FENE chain we cannot expect a scaling regime for $N = 100$ beads even without EVI as discussed in the previous section. As shown in Fig. 8 only for $N = 5000$ there is a small transition regime where the scaling predicted by the blob model applies for a freely jointed chain. With EVI there is the additional complication that at equilibrium the end–to–end distance with EVI is larger than without EVI but the deformation for large flow velocities is the same in both cases. Therefore the difference between the end–to–end distance at equilibrium and in the fully stretched state is smaller with than without EVI. and the slope of the $R_E(v)$ curves becomes smaller than without EVI. Thus it is expected that even longer chains are necessary to exhibit the blob scaling in the case with EVI if this is possible at all.

The discussion of the transverse extension of the polymer will be continued in the next section where we investigate the influence of both EVI and hydrodynamic interaction for a FENE chain.

5 Hydrodynamic Interaction

Throughout the previous three sections we have focused on polymer models where the hydrodynamic interaction (**HI**) between the beads has been neglected. The HI is more involved than the other interactions considered in this work and crucial for an understanding of the deformation of polymers in flow [19,20]. Furthermore it makes the coupling between polymers and solvent two–ways because it induces a perturbation of the imposed flow field due to the motion of the polymer. In this section we consider both Gaussian and FENE chains but we always take into account the EVI discussed in the previous section. For both models we then compare results without and with HI. In previous publications HI effects for tethered polymers have been considered either for blob models [59, 61] or for bead spring models but in the latter case only with averaged HI and discarding the EVI [62].

Fig. 14 shows the end–to–end distance as obtained from simulations of a bead spring chain with $N = 100$ harmonic springs. The upper curve is the same as the upper curve in Fig. 11 while the lower curve has been calculated with the HI between the segments taken into account as well.

The two curves are expected to approach each other both for vanishing and for very large flow velocities. At $v = 0$ both curves must coalesce because the HI change only the kinetic coefficient in the equation of motion and thus do not affect the static properties of polymers in thermal equilibrium [2,32]. For large velocities the polymer becomes uncoiled. Therefore the mean distance between beads that are far apart along the chain increases and the effects of HI are reduced. In addition each harmonic spring of the Gaussian chain is strongly stretched – approximately by a factor of 10 at $v = 1.0$ – and the dis-

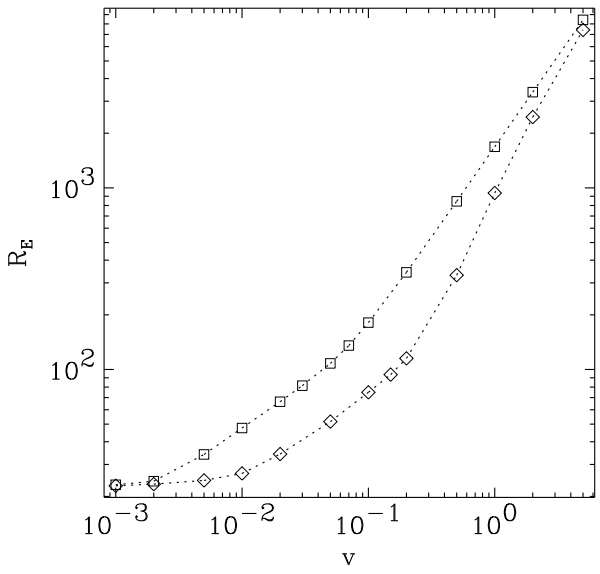

Fig. 14. End–to–end distance R_E as a function of the flow velocity v obtained from numerical simulations of a chain with $N = 100$ beads connected by harmonic springs with (lower curve) and without (upper curve) hydrodynamic interactions. In both cases the excluded volume interaction has been taken into account. The curve for the case without HI agrees with the uppermost curve in Fig. 11.

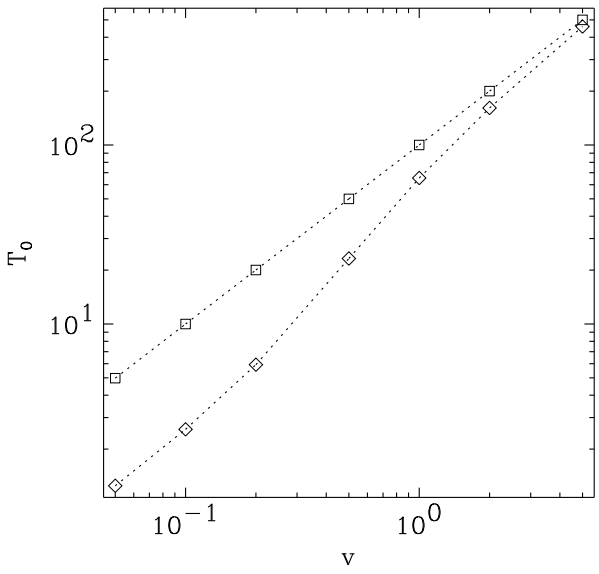

Fig. 15. Total drag force exerted on the polymer by the external flow, measured by the tension in the first spring T_0, as a function of the flow velocity v. The data have been obtained from numerical simulations of a chain with $N = 100$ beads connected by harmonic springs with (lower curve) and without (upper curve) hydrodynamic interactions. In both cases the excluded volume interaction has been taken into account. The upper curve is a linear function $T_0 \propto v$.

tance between neighboring beads in the chain increases, too. This effect reduces the HI further so that in the limit of very large flow velocities *all* beads are far apart from each other and the HI becomes completely negligible. In other words for large velocities the model with HI approaches the free–draining limit.

Between the limits of vanishing and very large flow velocities the elongation of the polymer is smaller with than without HI. In the velocity range $0.01 < v < 0.2$ (for $N = 100$) the end–to–end distance for the model with HI (lower curve in Fig. 14) has the same scaling as in the free–draining limit (upper curve). For larger velocities the slope of the curve with HI has to become larger than that without HI to approach the curve without HI in the limit of very large velocities. But even its maximum slope around $v \simeq 0.2$ corresponding to a power law $R_E \propto v^{1.5}$ is still considerably smaller than the exponent of 2 as predicted by the blob model with HI and EVI [59]. For a chain with $N = 200$ the maximum slope does not increase significantly (cf. Fig. 17 and Ref. [70]).

In order to understand this deviation it is illuminating to first discuss another aspect of HI. Fig. 15 shows the velocity dependence of the drag force exerted on the whole polymer chain which can be measured by the tension in the first spring. In the free–draining limit the total drag force is just the sum of the Stokes forces acting on each bead which are all proportional to the flow velocity v. Therefore the tension in the first spring grows linearly with the flow velocity as shown by the upper curve of Fig. 15. For a polymer with HI the total drag force $T_0(v)$ depends on the shape of the polymer and is therefore a nonlinear function of v as shown by the lower curve in Fig. 15. The quotient T_0/v defines a drag coefficient for the chain as a whole. In the free–draining case we simply have $T_0/v = N\zeta$ while with HI the drag coefficient T_0/v is no longer independent of v.

It is noteworthy that the drag force for the model with HI is always smaller than that in the free–draining case. This can be understood qualitatively as a consequence of the so-called non–draining effect, *i.e.* the screening of the flow field inside the polymer coil. As a result only the beads on the "surface" of the coil experience a Stokes drag. Since this is only a fraction of all beads the total drag force on the polymer is reduced compared to the free–draining case. With increasing flow velocity the polymer becomes more and more unwound which means that more beads are exposed to the flow. Alternatively we may say that the density of polymer segments is reduced which also reduces the strength of the HI or the screening of the flow field respectively. This weakening of the HI begins to become important at the flow velocity where the curves with and without HI in Fig. 14 cease to be approximately parallel, *i.e.* at $v \simeq 0.2$ for $N = 100$. It occurs first at the fixed chain end where the stretching of the chain is strongest. Then it increases and spreads out towards the free chain end. Since for a chain with harmonic springs the mean distance even between neighboring beads increases the HI

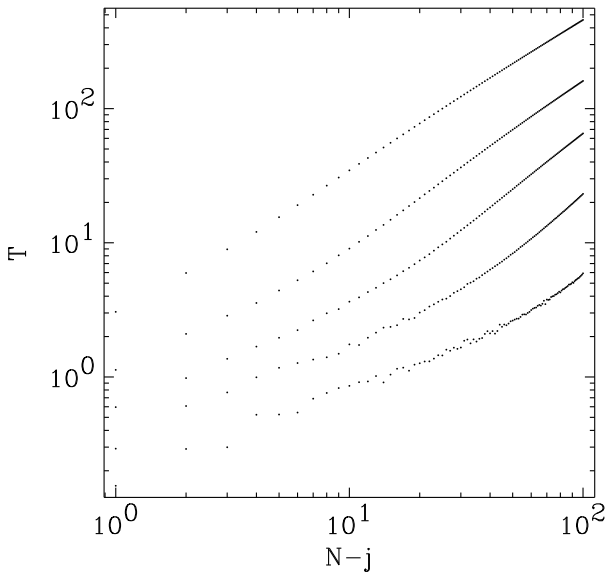

Fig. 16. Tension within the chain as a function of the bond index $N-j$ counted from the free chain end for different values of the flow velocity $v = 0.2$, 0.5, 1.0, 2.0, 5.0 from bottom to top. The data have been obtained from numerical simulations of a chain with $N = 100$ beads connected by harmonic springs with excluded volume and hydrodynamic interactions. For the largest velocity (uppermost curve) the tension is almost proportional to the bond index indicating that only the harmonic spring forces are effective.

between them finally becomes negligible as explained in the discussion of the chain elongation. Therefore also the drag forces with and without HI converge for large flow velocities.

The scaling behavior predicted for the total drag force by the blob model with EVI and HI is $T_0 \propto v^3$ according to the formulae given in Ref. [59]. Simulation data for a bead spring model with $N = 100$ shown in Fig. 15 give a maximum slope of 1.5 for the $T_0(v)$ curve around $v \simeq 0.2$. This exponent increases slightly to $t_0 \propto v^{1.6}$ for $N = 200$ (cf. Ref. [70]). It is very unlikely that the large discrepancies between both models with respect to the total drag force T_0 are solely due to finite size effects. We suspect that the conditions assumed in the blob model are not fulfilled for the bead spring chain with HI. The blob model assumes impenetrable blobs all along the string of blobs [59]. However, according to our simulations it is more likely that the polymer is neither free–draining nor non–draining as assumed previously but that a partial draining occurs instead as shown by directly calculating the perturbed velocity field in Ref. [70]. Furthermore similarly to the EVI also the strength of HI varies along the chain. This spatial variation of both effects is not represented in the free– and non–draining blob models (cf. appendix A and [59]). The variation of the effective HI may be taken into account qualitatively by a modification of the blob model that interpolates between both limits as described in Refs. [70, 90].

A clue to the inhomogeneous effects of HI is given by the local tension along the polymer. In Fig. 16 we show the tension T_{N-j} in bond $N-j$ for different flow velocities for a chain with $N = 100$ beads. In the free–draining case without EVI T_{N-j} is a linear function of j because each bead experiences the same drag force ζv and the forces on all beads starting from the free chain end add up to the tension in the j–th bond. Therefore a power law $T_{N-j} \propto N-j$ in the curves in Fig. 16 indicates that the corresponding part of the chain is free–draining. For $v = 5.0$ (uppermost curve in Fig. 16) this is roughly the case for the whole chain. For smaller flow velocities the tension increases with a slope larger than 1 close to the fixed end where the polymer becomes more and more uncoiled. Because of the uncoiling the HI becomes weaker and the effective drag on each bead increases when the fixed end is approached resulting in an increase of the tension with a slope larger than one. Near the free end the slope of the T_{N-j} curves is reduced due to EVI effects as discussed in section 4 but the actual value of the slope, 0.63 for $v = 0.02$ (lowest curve in Fig. 16), is now modified by HI.

In order to compare chains of different lengths Nb we plot the fractional extension versus the total drag force T_0 in Fig. 17. In the free–draining limit considered in the previous sections the total drag force was simply proportional to the flow velocity v. When HI is included the drag force depends on the polymer conformation. As Fig. 15 shows it does not obey a simple power law dependence on v. Using the numerical data for T_0 we again find that the curves for different N collapse on a single master curve as shown in Fig. 17. Note that the range of drag forces in Fig. 17 does not extend to values as small as in Fig. 12 and Fig. 8 because data for T_0 corresponding to smaller flow velocities have a rather large statistical error. Therefore the near–equilibrium regime where the curves fall apart is not visible in Fig. 17.

Finally we turn to the transverse extension of the Gaussian chain with EVI and HI. At the same flow velocity polymers with HI are less elongated in flow direction than free–draining polymers (cf. Fig. 14). Assuming that the bead spring chain occupies roughly the same volume with and without HI one may expect that the extension of a polymer perpendicular to the flow direction is larger for a chain with HI than without. The mean transverse component of the gyration tensor defined in Eq. (12) is a reasonable measure to test this conjecture. In Fig. 18 we show these data calculated from simulations of a Gaussian chain with EVI and both with and without HI. A large part of the curves at small to medium flow velocities confirms this expectation. However, the regime at large velocities where the chain with HI is contracted transversely compared to that without HI shows that the effects of HI are not always obvious. Hence situations where HI is potentially important should be considered with care. At very large flow velocities both curves converge towards the value for

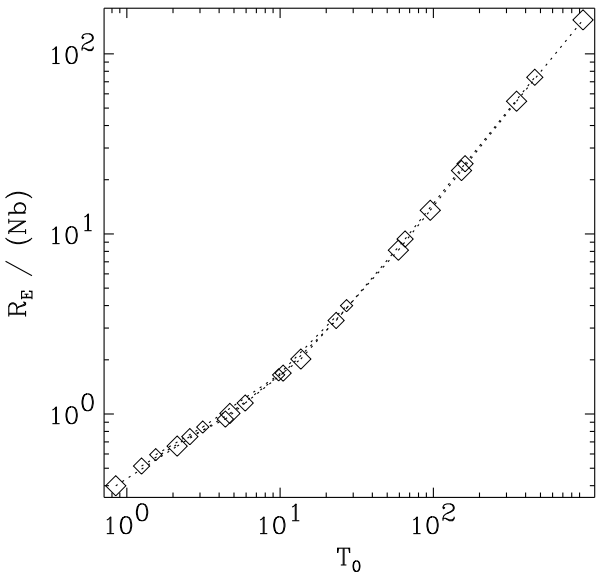

Fig. 17. Normalized end–to–end distance $R_E/(Nb)$ for chains of different lengths $N = 50, 100, 200$ (small, medium and large diamonds) as functions of the total drag force acting on the chain. The model considered here assumes harmonic springs and both excluded volume and hydrodynamic interactions are taken into account. Because of the presence of the excluded volume interactions the effective bond length is $b = 1.37$ (cf. appendix E). The total drag force is measured by the tension in the first spring (cf. Fig. 15). In the free–draining case the total drag force is just N times the single bead friction coefficient ζ, while in the case with HI considered here it is not known analytically. The relation between T_0 and v is shown in Fig. 15 for $N = 100$.

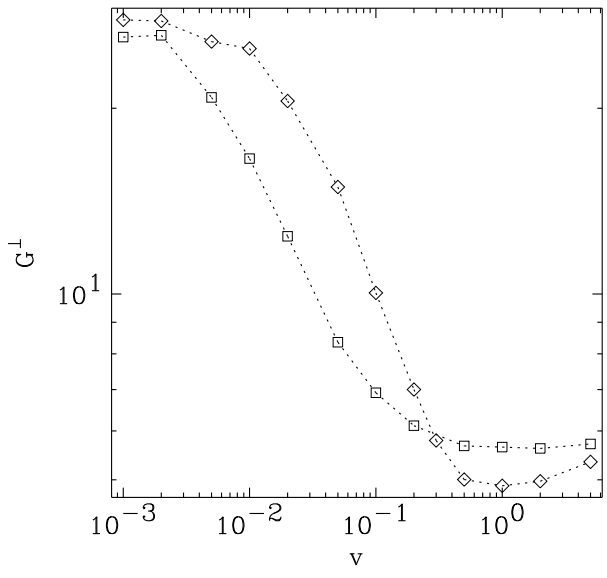

Fig. 18. Transverse component of the gyration tensor $G^\perp$ as a function of the flow velocity v for a chain with $N = 100$ beads connected by linear springs with (diamonds) and without (squares) hydrodynamic interactions. Excluded volume interactions are taken into account in both cases. For a Gaussian chain with $N = 100$ beads is $G^\perp = 5.56$ independent of the flow velocity, cf. Eq. (13).

the Gaussian chain which is $G^\perp = 5.56$ independent of v according to Eq. (13).

The flow velocity dependence of the end–to–end distance for a FENE chain with EVI and a FENE chain with both EVI and HI is compared in Fig. 19. As in the case of harmonic springs the elongation of the chain is shifted towards larger flow velocities when HI is included. Because of the limited attainable chain lengths we do not expect to observe a power law behavior at moderate flow velocities. Both curves do not end in a plateau with $R_E = Nb = 100$ at large flow velocities but continue to grow according to a power law with some small exponent because of the residual stretchability of the FENE springs discussed in section 3.

As far as the drag force is concerned chains with finite extensibility show a major difference compared to the Gaussian chain when HI is included. For a Gaussian chain the HI between the beads is reduced with increasing flow velocity for two reasons: Unwinding of the chain increases the distance between beads that are far apart along the chain and stretching of each spring also increases the distance between neighboring beads as discussed before. For a freely jointed chain the segment length is fixed and the

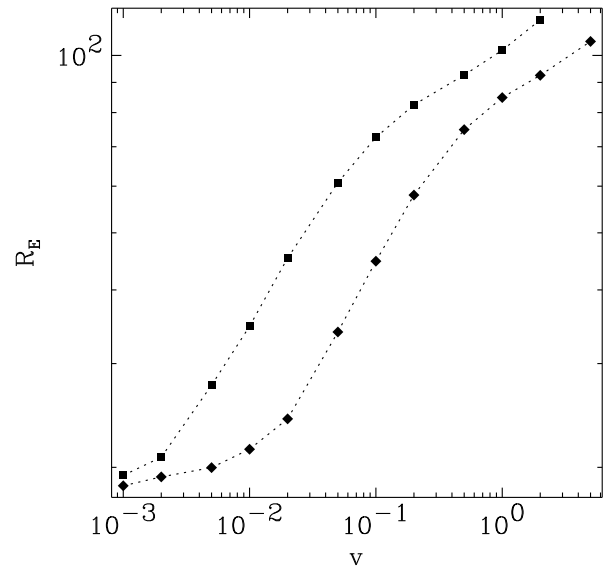

Fig. 19. End–to–end distance R_E as a function of the flow velocity v obtained from numerical simulations of a FENE chain with $N = 100$ beads with (lower curve) and without (upper curve) hydrodynamic interactions. In both cases the excluded volume interaction has been taken into account.

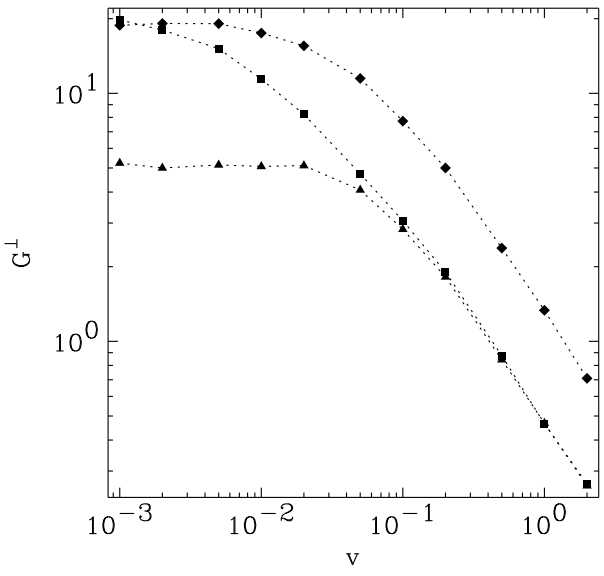

Fig. 20. Transverse component of the gyration tensor $G^\perp$ for a chain with $N = 100$ beads connected by FENE springs as a function of the flow velocity v without further effects (triangles), with excluded volume interactions only (squares) and with both excluded volume and hydrodynamic interactions (diamonds).

second mechanism is absent. Therefore neighboring beads stay rather close at any flow velocity and hence the effects of HI between neighboring beads are present even in the fully uncoiled state where the chain resembles a straight line. For this model the curves for the tension $T_0(v)$ in the free–draining limit and with HI become parallel but they never merge. Therefore the variation of the total drag force with the flow velocity that one can expect for the freely jointed chain is smaller than that for the chain with harmonic springs. For FENE chains this behavior may be slightly softened due to the residual extensibility of the FENE springs.

The comparison of the results for the total drag force obtained from simulation of a FENE chain with EVI only and with both EVI and HI showed that at small flow velocities, *i.e.* $v = 0.1$ for $N = 100$, HI reduces the drag by an amount which is twice as large as for the chain with harmonic springs. However, in contrast to the chain with harmonic springs (cf. Fig. 15) this difference remained constant over the whole range of flow velocities considered. Probably much longer chains than $N = 100$ are needed to exhibit that variation in the drag force which is solely due to the unwinding of the polymer.

The values of the transverse component of the gyration tensor $G^\perp$ for the FENE chain with only EVI and with both EVI and HI are shown by the two upper curves of Fig. 20. In contrast to the chain with harmonic springs $G^\perp$ is now larger with HI than without for *all* values of the flow velocity. Comparing these two cases to the case with neither EVI nor HI (lower curve in Fig. 20) we find a power law behavior with the same exponent $G^\perp \propto v^{-0.8}$ in all three cases when the flow velocity v is large enough.

In comparison to the predictions of the blob model we find agreement in so far as the exponent is independent of the EVI when HI are neglected. The different value of $G^\perp \propto v^{-1}$ for the blob model may be ascribed to the residual stretchability of the FENE chain as discussed in section 3. However, the blob model predicts a behavior as $v^{-1/\nu}$ in the non–draining case while the simulation data give a value which is still independent of the presence of EVI even when HI are included, too. This confirms the doubts already expressed in section 3 about the validity of the blob model as far as the transverse extension of the polymer is concerned.

6 Discussion and conclusions

We have investigated bead spring models and blob models for a single polymer which is fixed at one end and exposed to a uniform flow. The bead spring model is a standard model for the investigation of the long-time dynamics of polymers, while the blob model is a more coarse grained model which is appealing because of its simplicity. Both types of models are analyzed for different interactions between the polymer segments. Their scaling properties are compared to each other and to recent experiments on the same problem.

For the simplest case of the bead spring model the beads are connected by either linear or nonlinear springs – where the latter restrict the extensibility of the chain – and all other effects are neglected. This model is gradually completed by taking into account further effects such as the excluded volume interaction (**EVI**) and finally the hydrodynamic interaction (**HI**). The HI results in a perturbation of the external flow which modifies the drag experienced by the individual beads relative to the free–draining case where each bead experiences the same Stokes drag caused directly by the unperturbed external flow. For the simpler cases without EVI and HI analytical results have been obtained which allow to draw conclusions about arbitrarily long chains. Furthermore they provide a test of the numerical simulations which are the only possibility to treat the more complicated cases.

Since the predictions of the blob model are scaling laws they are expected to hold only for very long chains. Previous blob models for a tethered polymer in uniform flow have considered only the non–draining limit [59], attempting to model a situation with strong HI. The possible chain length in simulations of bead spring models, however is most severely restricted by the HI. In order to make a comparison between scaling predictions of blob models and simulations of bead spring chains we have therefore derived a blob model for a free–draining polymer in appendix A. The scaling laws for this model are rather different from those for the non–draining blob model as shown in table 1 which summarizes the results for the various blob models together with the analytical results for the Gaussian chain.

model	L, R_E	$\rho(\tilde{x})$	$\Upsilon(\tilde{x})$
Gaussian	$v\,N^2$	$\tilde{x}^{-\frac{1}{2}}$	
Blob (fd) $\nu=\frac{1}{2}$	$v\,N^2$	$\tilde{x}^{-\frac{1}{2}}$	$\tilde{x}^{-\frac{1}{2}}$
Blob (fd) $\nu=\frac{3}{5}$	$v^{\frac{2}{3}}N^{\frac{5}{3}}$	$\tilde{x}^{-\frac{2}{3}}$	$\tilde{x}^{-\frac{3}{5}}$
Blob (nd) $\nu=\frac{1}{2}$	$\exp\left(\frac{vN\eta b^2}{k_BT}\right)/\sqrt{v}$	$\tilde{x}^{-1}$	$\tilde{x}^{-1}$
Blob (nd) $\nu=\frac{3}{5}$	v^2N^3	$\tilde{x}^{-\frac{2}{3}}$	$\tilde{x}^{-1}$

Table 1. Scaling relations for various quantities describing the extension and shape of a tethered polymer in a uniform flow field. L, $\rho(\tilde{x})$ and $\Upsilon(\tilde{x})$ are extension and segment density in the flow direction and the envelope perpendicular to the flow direction where $\tilde{x}$ measures the distance from the free end of the polymer. These quantities are calculated for the free–draining (fd) blob model in appendix A and for the non–draining (nd) blob model in Ref. [59]. The end–to–end distance R_E and the segment density $\rho(\tilde{x})$ for the Gaussian chain are calculated in appendix B.

In thermal equilibrium the scaling relation between the end–to–end distance and the number of Kuhn segments, $R_E \propto N^\nu$ with $\nu = 1/2$ or $3/5$, is independent of the force law of the springs connecting consecutive segments. If the chain is exposed to a flow field, however, the end–to–end distance at a certain flow velocity are rather different for Gaussian chains and chains with finite extensibility. The reason is that the harmonic springs of a Gaussian chain are strongly stretched (cf. section 2 and appendix B) while for a FENE chain there is only a weak stretching of individual springs at very large flow velocities as discussed in section 3 and for the freely jointed chain there is no stretching at all. Since the blob model is based on the equilibrium scaling (cf. appendix A) it does not distinguish between these cases. The use of a fixed bond length b in all blobs suggests, however, that it is more in the spirit of the model to compare it to a freely jointed chain. In fact, real polymers are best modelled as freely jointed chains for a wide range of parameters since the chemical bonds possess a definite length. This is also the case for DNA [91, 92]. However, even though the Gaussian chain is not a very realistic model for polymers in external fields, due to its simplicity, it nevertheless provides a convenient test case for the blob model which formally uses the same premises.

The analytical scaling laws for blob models as summarized in table 1 are obtained by an approximate solution (cf. appendix A) of the model equations. An exact numerical solution of the latter reveals a behavior of the polymer extension which is more complex than a simple power law as shown in Fig. 22 for the free–draining blob model. Only for very long chains does the scaling of the polymer extension $L(v)$ come close to a power law in a small velocity range. For the non–draining blob model the deviations between the power law derived from the analytical approximation and the behavior obtained from the exact numerical solution are even larger [90]. Accordingly a perfect power law behavior of the end–to–end distance $R_E(v)$ for beads spring models may not be expected in general.

In section 2 we compared the Gaussian chain, *i.e.* a bead spring chain with harmonic springs and no other interactions between the beads, to the free–draining blob model without EVI, *i.e.* with Flory exponent $\nu = 1/2$. As shown in Fig. 3 there is perfect agreement between the scaling of the end–to–end distance for the bead spring–model and the in-flow extension as calculated for the free–draining blob model, $L \sim R_E \propto v$, when the flow velocity is larger than some threshold which marks the onset of the so-called trumpet regime [61]. Also the power law for the segment density $\rho \propto (x_0 - x)^{-1/2}$ predicted by the blob model is in good agreement with results for the bead spring model (cf. Fig. 4). However, in the case of harmonic springs there is no upper limit for the validity range of the trumpet regime because the elongation of the chain is caused by a stretching of the individual bonds which can grow without bounds.

For the freely jointed chain in contrast any stretching of individual bonds is forbidden and the mechanism by which the elongation occurs is solely an unwinding of the chain. It was verified in section 3 that the freely jointed chain is well approximated by a FENE chain provided the flow velocity is not extraordinarily large. The dependence of R_E on the flow velocity v is not a simple power law for these models. A certain scaling regime exists but it is confined to a small range of flow velocities and the exponent of the blob model is approached only for very long chains ($N \gtrsim 5000$) as shown in Fig. 8. The segment density turned out to be a bad discriminator between the trumpet and the stem and flower regimes.

EVI reduces the slope of the $R_E(v)$ curves. In section 4 (cf. Fig. 11) we found a slope of 0.5 for the bead spring model with harmonic springs at medium values of the flow velocity, where EVI are expected to be important. At larger flow velocities the EVI becomes unimportant and a crossover to a slope of 1.0 characteristic of the case without EVI occurs. The slope of 2/3 predicted by the free–draining blob model with the Flory exponent $\nu = 3/5$ characteristic for EVI is somewhat larger than that obtained in the simulations. One reason for this discrepancy might be that the chains with $N \leq 200$ used in our simulations are too short. However, for the Gaussian chain good agreement was obtained in the case without EVI for a chain length of only $N = 100$. A probably more important cause of the discrepancy between the blob and bead spring models with EVI is a fundamental deficiency of the blob model in this case. Because the polymer is stretched stronger close to the tether point than near the free end for the bead spring model and also for real polymers the effects of EVI are not homogeneous over the whole chain (cf. Fig. 13). In the blob model, however, EVI enters only via the Flory exponent $\nu = 3/5$ which is the same in all blobs.

Finally in section 5 the effects of HI between the beads are taken into account in addition to the EVI. The HI shifts the elongation of the polymer to larger flow velocities as indicated in Fig. 14 and Fig. 19. In other words the drag force for a given velocity of the uniform flow is smaller in the case with HI between polymer segments

than without (cf. Fig. 15). For moderate flow velocities v the slopes of the $R_E(v)$ curves with and without HI in Fig. 14 agree in the case with harmonic springs which means that the deformation is dominated by EVI for the model parameters as given in Appendix E. For very large flow velocities in the case with harmonic springs *all* beads are separated due to the stretching of the chain and the HI become completely negligible. For a FENE chain in contrast the springs are at most slightly stretched and therefore HI between next–nearest neighbors remains unchanged when the flow velocity is increased. Therefore the drag force obtained for a free–draining chain is not approached in this case.

In both cases, with harmonic or FENE springs, there is an intermediate velocity regime where the slope of the $R_E(v)$ curves is larger with HI than without. However, this slope is always smaller than predicted for blob models with impenetrable blobs [59]. This has two reasons. Similar as the EVI also the effects of the HI depend on the local shape of the polymer. The crossover to free–draining behavior occurs already at smaller v near the tether point where the polymer is more unwound than close to the free end where it is still coiled up. This spatial dependence of HI effects is not taken into account in blob models. A second reason for the disagreement is discovered when the perturbation of the flow field caused by the polymer is calculated. From the perturbed flow field it can be seen that flow partially penetrates the polymer in contrast to the assumption of impenetrable blobs in the blob model [70].

These effects can be taken into account within a blob model as described in [70,90], where the so-called F-shell blob model has been introduced. For the F-shell blob model each blob consists of a free–draining outer shell (F-shell) and an impenetrable inner core. The thickness of the F-shell is assumed constant for all blobs but relative to the blob size it is deeper for the small ones which eventually become completely free–draining. This model therefore describes the transition between a nearly impenetrable polymer coil at small flow velocities and an almost free–draining stretched polymer at large flow velocities as observed in the numerical simulations presented in this work. The exponents predicted by the F-shell blob model are in good agreement with those obtained from the numerical simulations. The predictions of the blob model with impenetrable blobs may be considered as upper limits for the true ones.

In recent experiments with DNA the chains contained up to $N = 1600$ [39] and $N = 3000$ [62] Kuhn segments. As we have shown such chains are still too short to expect a scaling behavior as predicted by the blob model in the free–draining case and even less in reality when HI are important. Furthermore the analytic scaling relation for the polymer extension L is obtained by an approximate solution to the blob model which approaches the exact numerical solution only close to v_{c2}, the upper limit of the scaling regime, even for long chains (cf. Fig. 22). But in this velocity regime the polymer is already considerably elongated and it has been shown that at large elongations the semi-flexibility leads to a significant deviation from the behavior of a freely jointed chain [93,57]. Since this interaction is not included in the blob model the predicted scaling laws are of limited use for the quantitative understanding of the experiments on DNA. For use in a micro–rheological theory of polymers where only qualitative effects are important in a first step, the effect of semi-flexibility may be neglected and the blob model may be employed to obtain useful estimates.

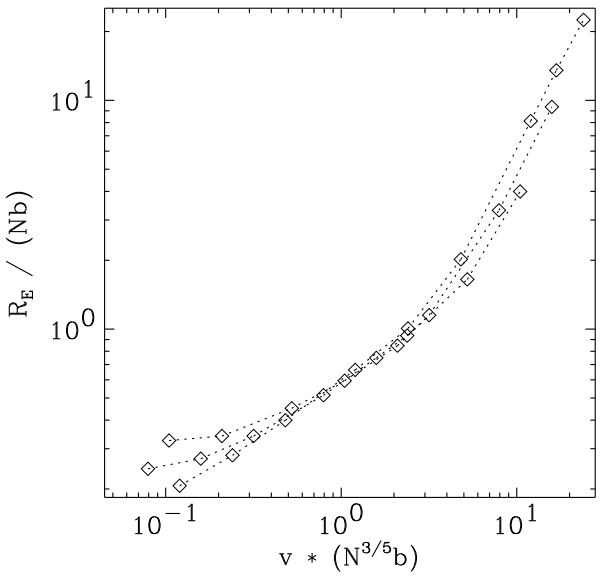

Fig. 21. Normalized end–to–end distance $R_E/(Nb)$ for chains of different lengths $N = 50, 100, 200$ as function of the reduced flow velocity $vN^{3/5}b$. The model considered here assumes harmonic springs and both excluded volume and hydrodynamic interactions are taken into account. Because of the presence of the excluded volume interactions the effective bond length is $b = 1.37$ (cf. appendix E).

The measured polymer elongation $R_E(v)$ [62] has a similar shape as shown in Fig. 19. For fitting this curve a half–dumbbell model has been used [62] with a phenomenological spring–force that was found to be in fairly good agreement with experiments on DNA molecules which are pulled at both ends [56,57,93] . With such a model one might fit the measured data but it gives only limited insight about the different mechanisms at work. For instance a model with only one bead and one spring cannot give much insight about the increasing penetration of flow into the polymer or about the spatial variation of the effects of EVI and HI along a deformed polymer.

A main focus of the experimental work [39,62] was to determine the extent to which HI is important depending on the flow velocity v. The criterion on which the judgement was based was the deviation from the data collapse which is expected for the free–draining limit when the fractional extension $R_E/(Nb)$ is plotted versus the total drag force $N\zeta v$ for different chain lengths Nb (cf. Eq. (4)). In Fig. ?? of Ref. [39] it was found that a data collapse

occurs when $R_E/(Nb)$ is plotted versus $vN^\nu\, b$. This finding was explained by the non–draining picture, *i.e.* the idea that strong HI makes the polymer coil behave like a solid object. This picture suggests that up to a logarithmic correction [94] the total drag force should scale as the largest linear extension of the coil. Instead of the true elongation $R_E(v,N)$ the equilibrium extension of the coil $R_E(0,N) \propto N^\nu\, b$ has been used in Ref. [39] to approximate the total drag force. A similar plot is shown in Fig. 21 where the fractional chain extension is plotted over $v(N^{3/5}\, b)$. The curves do approximately superimpose in the reduced velocity regime $vN^{3/5}\, b = 0.5 \ldots 3.0$. This corresponds to $v \simeq 0.03 \ldots 0.2$ for $N = 100$, *i.e.* the range in Fig. 14 where the curves with and without HI are approximately parallel. This is quite surprising since the chain is already significantly stretched in this velocity range and $R_E(0,N)$ is a quite bad approximation to the true linear dimension of the coil. In fact, our results in Fig. 17 show that when the *true* drag force is used the curves collapse over the whole range of flow velocities larger than some threshold. To explain the behavior observed in Fig. 21 there must be a compensating effect which just cancels the underestimation of the linear extension of the coil implied by the use of the equilibrium scaling for R_E. This maybe the neglect of the logarithmic correction which accounts for the ellipsoidal shape of the deformed polymer coil similar as the argument in [62].

The purpose of this work was an analysis of how the different interactions, the type of spring law, EVI, and HI play together at various stages of the polymer deformation. Here we have chosen for this purpose one special set of parameters in the bead spring models as given in appendix E. For comparison with results of specific experiments other parameters may be required which put more or less emphasize on the EVI or HI than in this work. For example for DNA molecules the EVI–effects are expected to be weaker than assumed in our simulations due to the large persistence length of DNA.

In this work we only considered the static deformation of a tethered polymer due to the presence of a uniform flow. Equally important is the perturbation of the imposed flow caused by the motion of the polymer. Taking into account the full fluctuating hydrodynamics (cf. appendices E and F) allowed for the first time to calculate this flow perturbation explicitly which has been presented in two preliminary notes [77,70]. The dynamics of the polymer will be described elsewhere. Since the equation of motion is strongly nonlinear one has to distinguish the relaxation of fluctuations at steady state [72] and the dynamics of mean values when the flow is suddenly turned on or off [71]. In the former case the *complete* relaxation spectrum can be obtained by applying the Karhunen–Loève method. The Brownian dynamics algorithm is presently generalized to shear flows which cannot be described by a velocity potential. In Poiseuille flow for instance an interesting migration effect has been found recently [95].

The case of a tethered polymer in uniform flow provides an especially simple model problem which facilitates the investigation of both the polymer deformation and the flow perturbation. It may serve as a starting point for developing improved coarse grained descriptions for polymers in flow similar to other fields in polymer physics [96]. Thus the comprehensive study of this model problem is one of the very first steps towards a well founded fluid dynamics of dilute polymer solutions. For a deeper understanding of the rheology of dilute polymer solutions it is important to also consider freely floating polymers in more realistic flow fields such as simple shear, Poiseuille and even turbulent flows. This task will be pursued further in the future.

It is a great pleasure to thank D. Kienle, S. Chu, H. Müller–Krumbhaar and V. Steinberg for useful discussions.

A Blob model for the free–draining limit

Blob models have been used to describe scaling properties of polymers in non–equilibrium situations [2] such as a single polymer pulled at both ends [63,64] and the case under consideration here, namely a single tethered polymer in a uniform external flow [59–61]. In the latter works impenetrable blobs were assumed modelling the effect of hydrodynamic interaction between the polymer segments. In this appendix we describe a similar scaling model for the free–draining limit where the external flow completely penetrates the polymer coil. We derive the expressions for the segment density, the integral extension of the polymer in the flow direction, and the lateral extension of the polymer. The results obtained here together with the relations derived in Refs. [59–61] for the non–draining blob model are summarized in table 1 and compared with results from different approaches in sections 2 through 4.

The blob model relies on two assumptions in order to describe a polymer in an external force field. The first assumption is that under the influence of the external force the equilibrium coil breaks up into a string of blobs as sketched in Fig. 1. The portion of the polymer chain within the k-th blob acts as an entropic spring that contains some tension T_k in the direction of the external force. The size of the k-th blob R_k is determined by a balance between the elastic energy of that spring $R_k T_k$ and the thermal energy for one degree of freedom. This is expressed by the Pincus rule [63,64]

$$\frac{k_B T}{R_k T_k} \approx 1\,. \tag{14}$$

Then within each blob the effects of the external force are small and it is justified to assume that the equilibrium scaling relations (see *e.g.* Refs. [2,31,32]) are still valid, *i.e.*

$$R_k = b N_k^\nu\,, \tag{15}$$

where N_k is the number of segments within the k–th blob and b is the Kuhn length. Taking the same value for b in each blob amounts to considering a freely jointed chain here. For a Gaussian chain in flow the individual segments

would be stretched as discussed in the following appendix and section 2 requiring an x–dependent segment length. The exponent ν depends on the solvent quality, *i.e.* $\nu = 3/5$ for a good solvent and $\nu = 1/2$ for a θ-solvent [2,31, 32,85].

Finally one needs to specify the tension T_k within each blob. This tension is given by the sum of the Stokes friction forces acting on all blobs starting from the free end ($k = 1$). In the free–draining limit the friction force on each blob is given by the sum of the friction forces $\eta a v$ acting on each of the segments within the blob. Here η, a and v are the viscosity of the solvent, the effective hydrodynamic radius of a segment and the magnitude of the flow velocity, respectively. We thus obtain for the tension

$$T_k \propto \eta a v \sum_{j=1}^{k} N_j \,. \tag{16}$$

Combining Eqs. (14)–(16), one finds the following recurrence relation for the tension in each blob:

$$T_k - T_{k-1} \propto \eta a v \left(\frac{k_B T}{b T_k}\right)^{\frac{1}{\nu}} . \tag{17}$$

This has to be supplemented by a boundary condition for the first blob which is obtained by noting that Eq. (16) gives $T_0 = 0$. Inserting this in Eq. (17) and solving for T_1 yields $T_1 \propto (\eta a v)^{\frac{\nu}{\nu+1}} (k_\mathrm{B}T/b)^{\frac{1}{\nu+1}}$. Eq. (17) together with this boundary condition is now a closed equation for the tension within the blobs.

Rewriting Eq. (17) in differential form by approximating $T_k - T_{k-1} \approx dT/dk$ one obtains a solution which is valid in the limit of large k:

$$T_k \propto \left(\eta a v\, k\right)^{\frac{\nu}{\nu+1}} \left(\frac{k_\mathrm{B}T}{b}\right)^{\frac{1}{\nu+1}} . \tag{18}$$

The position of the k-th blob $\tilde{x}_k$ is found from $\tilde{x}_k = \sum_{j=1}^{k} R_j$. Here $\tilde{x}$ is the x–coordinate measured from the free end of the chain x_0, *i.e.* $\tilde{x} = x_0 - x$.

Using Eq. (14) and replacing the sum by an integral, which is consistent with the approximation that lead to Eq. (18), one arrives at

$$\tilde{x}_k \propto \left(\frac{k_\mathrm{B}T}{\eta a v}\right)^{\frac{\nu}{\nu+1}} \left(b\, k\right)^{\frac{1}{\nu+1}} . \tag{19}$$

Eliminating the blob index k between Eq. (18) and Eq. (19) yields the law for the tension in the free–draining case,

$$T(\tilde{x}) \propto \frac{1}{b} \left(k_\mathrm{B}T\right)^{1-\nu} \left(\eta a v \tilde{x}\right)^{\nu} . \tag{20}$$

The corresponding relation for the non–draining case is [59],

$$T(\tilde{x}) \propto \eta v \tilde{x} \,, \tag{21}$$

which is derived in a similar manner by using the relation $T_k \propto \eta v \sum_{j=1}^{k} R_j$ in place of Eq. (16).

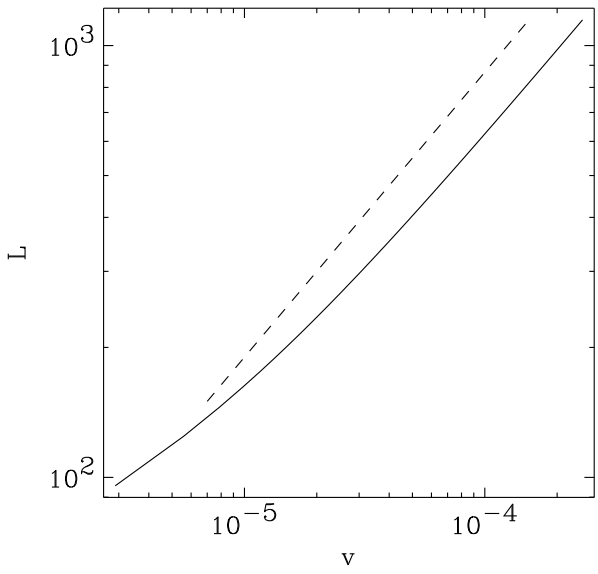

Fig. 22. In–flow extension L as obtained by numerically solving the recursion relation Eq. (17) and summing up all blob radii R_k according to Eq. (14) for a free–draining blob model $N = 2000$ beads (solid curve) and $\nu = 3/5$ corresponding to the case with exluded volume interaction. The dashed line is the power law obtained by the approximate analytical solution Eq. (23).

An expression for the segment density projected onto the x-axis $\rho(\tilde{x})$ follows from $\rho \approx N_k/R_k$ by using Eqs. (14)–(15) and replacing T_k by $T(\tilde{x})$:

$$\rho(\tilde{x}) \propto \frac{1}{b} \left(\frac{\eta a v}{k_\mathrm{B}T}\right)^{\nu-1} \tilde{x}^{\nu-1} . \tag{22}$$

The integral extension L of the chain in x–direction follows from the normalization requirement $\int_0^L d\tilde{x}\, \rho(\tilde{x}) = N$, where N is the total number of segments in the whole polymer chain. The result is

$$L \propto \left(\frac{\eta a v}{k_\mathrm{B}T}\right)^{\frac{1-\nu}{\nu}} (N b)^{\frac{1}{\nu}} . \tag{23}$$

From Eq. (23) together with Eq. (20) one obtains $T(L)$ as a measure of the total drag force exerted on the polymer. For the free–draining case the result is $T(L) = \eta a v N$ as expected (cf. section 2). The extension $\Upsilon(\tilde{x})$ of the chain perpendicular to the flow direction is obtained from $\Upsilon \approx R_k$ as

$$\Upsilon(\tilde{x}) \propto b \left(\frac{k_\mathrm{B}T}{\eta a v}\right)^{\nu} \tilde{x}^{-\nu} . \tag{24}$$

There are obvious restrictions on the validity of the blob model. First of all the polymer chain may be modelled as a string of blobs only in a certain range of velocities $v_{c1} < v < v_{c2}$, the so-called trumpet regime [61]. The reason is simply that the radius of the blob close to the free

end as determined by the Pincus rule must not be larger than the Flory radius for the whole chain R_F. On the other hand the smallest blob at the fixed end cannot be smaller than the segment length b. The first situation may occur in very weak flows and the second in very strong flows. The limiting velocities v_{c1} and v_{c2} for the free–draining case are

$$v_{c1} = \frac{k_B T}{\eta a b N^{\nu+1}} \qquad \text{and} \qquad v_{c2} = \frac{k_B T}{\eta a b N}\,, \tag{25}$$

where the ratio between both velocities depends on N as

$$v_{c2} = N^{\nu}\, v_{c1}\,. \tag{26}$$

For the non–draining case one has [61]

$$v_{c2} = N^{\frac{1}{5}}\, v_{c1}\,. \tag{27}$$

The rather weak N–dependence of the ratio v_{c2}/v_{c1} shows that very long chains will be needed to obtain a significant range for the scaling laws derived in Eqs. (22)–(24).

Furthermore Eq. (18) is derived for large values of the blob index k and therefore the derived scaling behavior may not hold close to the free end of the polymer where k is small. To achieve both large values of k and a considerable number of segments N_k within the k-th blob one needs very long chains. Only then the scaling behavior as calculated above can be expected for some range of flow velocities. To get an estimate on the required chain length we compare in Fig. 22 the chain extension L as a function of flow velocity v for the free–draining blob model with $\nu = 3/5$ and $N = 2000$ beads as obtained by numerical evaluation of the exact recursion relation Eq. (17) to the scaling law obtained by the approximation Eq. (18). It is clear that even at this chain length the scaling regime is not yet visible. The comparison between the analytical scaling result and the numerical solution of the recursion relation is even less fortunate for non–draining blob models as described elsewhere [90]. Accordingly scaling results may be considered as upper limits for the slope of $L(v)$ only.

B Gaussian chain

Static properties of flexible polymers in thermal equilibrium can be calculated from the conformational distribution function [31,32]. In this appendix we consider a bead spring model as sketched in Fig. 2 where we assume harmonic springs and the binding between consecutive beads is the only interaction that is taken into account. For this model we calculate several static properties of a tethered polymer in uniform flow.

A potential for the harmonic springs is given by

$$\Phi^{\mathrm{H}}(\mathbf{Q}_j) = \frac{1}{2}\,\frac{3k_{\mathrm{B}}T}{b^2}\,|\mathbf{Q}_j|^2\,, \tag{28}$$

where $\mathbf{Q}_j = \mathbf{R}_{j+1} - \mathbf{R}_j$ is the j–th bond vector and $\mathbf{R}_j$ is the position vector of bead j. The Boltzmann factor for the potential in Eq. (28) $\exp(-\Phi^{\mathrm{H}}/k_{\mathrm{B}}T)$ gives a Gaussian distribution for the bond lengths with a mean square bond length of b in thermal equilibrium (see *e.g.* Ref. [31,32]).

The uniform flow field is taken in the x–direction

$$\mathbf{v} = v\,\hat{\mathbf{x}}\,, \tag{29}$$

with $\hat{\mathbf{x}}$ the unit vector and v the magnitude of the flow velocity. The drag force acting on each of the beads is $\zeta\mathbf{v}$ where the friction coefficient ζ is given by Stokes formula $\zeta = 6\pi\eta a$ with η the solvent viscosity and a the effective hydrodynamic radius of a bead. For the flow given by Eq. (29) the drag force can be derived from a potential

$$U(\mathbf{r}) = -\zeta v\,\mathbf{r}\cdot\hat{\mathbf{x}}\,. \tag{30}$$

Keeping the first bead of the polymer chain fixed at the origin, the conformational distribution function reads

$$P(\{\mathbf{R}_j\}) = \delta(\mathbf{R}_0)\left(\frac{3}{2\pi b^2}\right)^{\frac{3}{2}N} \times \exp\!\left(\frac{1}{k_{\mathrm{B}}T}\sum_{j=1}^{N}\Phi^{\mathrm{H}}(\mathbf{Q}_j) + U(\mathbf{R}_j)\right)\,. \tag{31}$$

With the relation $\sum_{j=0}^{N}\sum_{i=0}^{j-1}\mathbf{Q}_i = \sum_{k=0}^{N-1}(N-k)\,\mathbf{Q}_k$ the distribution function can be simplified to

$$P(\mathbf{R}_0,\{\mathbf{Q}_j\}) = \delta(\,\mathbf{R}_0\,)\left(\frac{3}{2\pi b^2}\right)^{\frac{3}{2}N} \times \exp\!\left(-\frac{3}{2b^2}\sum_{j=0}^{N-1}|\mathbf{Q}_j - \mathbf{S}_j|^2\right)\,, \tag{32}$$

where

$$\mathbf{S}_j = \frac{\beta v b^2}{3}\,(N-j)\,\hat{\mathbf{x}} \qquad \text{and} \qquad \beta = \frac{\zeta}{k_{\mathrm{B}}T}\,. \tag{33}$$

We call $\mathbf{Q}_j - \mathbf{S}_j$ the stretched bond vector. It is now a straight forward task to determine all quantities of interest from this distribution function.

B.1 Mean bond vectors and mean square bond lengths

The calculation is most efficiently organized by first determining the first and second moments of the distribution of the bond vectors $P(\mathbf{Q}_k)$. For the components of the mean bond vector $\langle\mathbf{Q}_k\rangle$ we obtain

$$\langle Q_k^x\rangle = \left(\frac{3}{2\pi b^2}\right)^{\frac{3}{2}N}\int d^3\mathbf{Q}_0\,\ldots\,d^3\mathbf{Q}_{N-1}\;\mathbf{Q}_k\cdot\hat{\mathbf{x}} \times\exp\!\left(-\frac{3}{2b^2}\sum_{j=0}^{N-1}|\mathbf{Q}_j-\mathbf{S}_j|^2\right) = \frac{\beta v b^2}{3}\,(N-k)\,, \tag{34}$$

while the other components must vanish for symmetry reasons, *i.e.*

$$\langle Q_k^y \rangle = \langle Q_k^z \rangle = 0\,. \tag{35}$$

Similarly we find for the diagonal components of the covariance $\langle \mathbf{Q}_k \mathbf{Q}_k^T \rangle$

$$\left\langle (Q_k^x)^2 \right\rangle = \frac{b^2}{3} + \left(\frac{\beta v b^2}{3} \, (N-k) \right)^2 \tag{36}$$

$$\left\langle (Q_k^y)^2 \right\rangle = \left\langle (Q_k^z)^2 \right\rangle = \frac{b^2}{3}\,, \tag{37}$$

while the off-diagonal components again must vanish due to symmetry.

From these expressions all other quantities of interest are easily found, *e.g.* the mean square length of the k–th bond

$$\begin{aligned} \left\langle |\mathbf{Q}_k|^2 \right\rangle &= \left\langle (Q_k^x)^2 \right\rangle + \left\langle (Q_k^y)^2 \right\rangle + \left\langle (Q_k^z)^2 \right\rangle \\ &= b^2 + \left(\frac{\beta v b^2}{3} \, (N-k) \right)^2 . \end{aligned} \tag{38}$$

This expression shows that for the Gaussian chain the bonds close to the fixed chain end are considerably stretched under the action of a flow. On the other hand the mean square length of the bonds close to the free end has the same value b as in thermal equilibrium.

B.2 Mean bead positions, end–to–end distance and end–to–end tensor

The mean x–position of the k–th bead $\langle X_k \rangle$ is simply the sum over the x–components of the first k bond vectors (cf. Eq. (34)), *i.e.*

$$\langle X_k \rangle = \sum_{j=0}^{k-1} \langle Q_j^x \rangle = \frac{\beta v b^2}{3} \, \frac{2N-k+1}{2} \, k\,, \tag{39}$$

whereas the y– and z–components of the mean bead positions again must vanish.

For $k = N$ we obtain the mean end–to–end vector $\langle \mathbf{R}_N - \mathbf{R}_0 \rangle = (X_E, Y_E, Z_E)^T$. Its second moment is the end–to–end tensor E for the components of which we find

$$\begin{aligned} E^{\alpha\beta} &= \left\langle (\mathbf{R}_N - \mathbf{R}_0)(\mathbf{R}_N - \mathbf{R}_0)^T \right\rangle \\ &= \frac{b^2}{3} \, N \, \delta_{\alpha\beta} + \left(\frac{\beta v b^2}{3} \, \frac{N\,(N+1)}{2} \right)^2 \delta_{\alpha x} \, \delta_{\beta x}\,. \end{aligned} \tag{40}$$

The trace of the end–to–end tensor is the square of the familiar end–to–end distance

$$\begin{aligned} R_E^2 &= \left\langle |\mathbf{R}_N - \mathbf{R}_0|^2 \right\rangle \\ &= b^2 N + \left(\frac{\beta v b^2}{3} \, \frac{N\,(N+1)}{2} \right)^2 . \end{aligned} \tag{41}$$

B.3 Gyration tensor

A further quantity that is often used to characterize the shape and size of a polymer is the gyration tensor. The latter is the second moment of the distribution of bead position vectors relative to the center–of–mass $\mathbf{R}_{CM} = 1/N \sum_{i=0}^{N} \langle \mathbf{R}_i \rangle$:

$$\begin{aligned} \mathsf{G} = & \frac{1}{N} \sum_{j=0}^{N} \left\langle (\mathbf{R}_j - \mathbf{R}_{CM}) \, (\mathbf{R}_j - \mathbf{R}_{CM})^T \right\rangle \\ = & \frac{1}{2N^2} \sum_{i,j=0}^{N} \left\langle (\mathbf{R}_j - \mathbf{R}_i) \, (\mathbf{R}_j - \mathbf{R}_i)^T \right\rangle . \end{aligned} \tag{42}$$

Expressing $(\mathbf{R}_j - \mathbf{R}_i) = \sum_{k=i}^{j-1} \mathbf{Q}_k$ in terms of bond vectors and counting the number of occurrences of each bond vector $\mathbf{Q}_k$ in the triple sum we find

$$\mathsf{G} = \frac{1}{2N^2} \sum_{k=0}^{N-1} (N-k-1) \, (N-k) \, \left\langle \mathbf{Q}_k \mathbf{Q}_k^T \right\rangle . \tag{43}$$

Since $\langle \mathbf{Q}_k \mathbf{Q}_k^T \rangle$ is diagonal so is G.

When the polymer is stretched under the action of a flow the behavior of G^{xx} as a measure for the in–flow extension of the polymer is not quite intuitive because G^{xx} is taken relative to the x–position of the center–of–mass which itself depends on the strength of the stretching flow. The transverse components, however, are good measures for the extension of the polymer transverse to the flow. For the Gaussian chain we obtain

$$G^{yy} = G^{zz} = \frac{1}{2N^2} \left(\frac{1}{3} N^3 + \frac{2}{3} N \right) \frac{b^2}{3}\,. \tag{44}$$

B.4 Segment density

The segment density $\rho(\mathbf{r})$ is defined as

$$\rho(\mathbf{r}) = \left\langle \sum_{k=0}^{N} \delta(\,\mathbf{r} - \mathbf{R}_k\,) \right\rangle . \tag{45}$$

Using the Fourier representation of the δ-function

$$\delta(\mathbf{r}) = \frac{1}{(2\pi)^3} \int d^3\mathbf{q} \, \exp(\,i\mathbf{q}\cdot\mathbf{r}\,)\,, \tag{46}$$

Eq. (45) becomes

$$\begin{aligned}\rho(\mathbf{r}) &= \delta(\,\mathbf{r}-\mathbf{R}_0\,) \\ &+\left(\frac{3}{2\pi b^2}\right)^{\frac{3}{2}N}\frac{1}{(2\pi)^3} \\ &\sum_{k=1}^{N}\int d^3\mathbf{q}\,d^3\mathbf{Q}_0\,\ldots d^3\,\mathbf{Q}_{N-1} \\ &\times\exp\!\left(i\mathbf{q}\cdot\left(\mathbf{r}-\sum_{j=0}^{k-1}\mathbf{Q}_j\right)\right) \\ &\times\exp\!\left(-\frac{3}{2b^2}\sum_{j=0}^{N-1}|\mathbf{Q}_j-\mathbf{S}_j|^2\right) \\ &=\delta(\,\mathbf{r}-\mathbf{R}_0\,) \\ &+\sum_{k=1}^{N}\frac{1}{(2\pi)^3}\int d^3\mathbf{q}\,\exp\!\left(i\mathbf{q}\cdot\left(\mathbf{r}-\sum_{j=0}^{k-1}\mathbf{S}_j\right)\right) \\ &\times\exp\!\left(-\sum_{j=0}^{k-1}\frac{b^2}{6}\,|\mathbf{q}|^2\right)\,.\end{aligned} \tag{47}$$

The final $\mathbf{q}$–integration provides the expression for the segment density of a Gaussian chain in a uniform flow field

$$\begin{aligned}\rho(\mathbf{r}) &= \delta(\,\mathbf{r}-\mathbf{R}_0\,) \\ &+\sum_{k=1}^{N}\left(\frac{3}{2\pi k b^2}\right)^{\frac{3}{2}}\exp\!\left(-\frac{3}{2kb^2}\;(\mathbf{r}-\langle\mathbf{R}_k\rangle)^2\right)\,.\end{aligned} \tag{48}$$

This is a sum of Gaussian distributions centered about the mean position of the k–th segment $\langle\mathbf{R}_k\rangle$ with components given by Eq. (39). The explicit shape of $\rho(x)$ is obtained by numerically evaluating the sum in Eq. (48). It can be approximated by the simple power law as discussed in section 2.

B.5 Quasi–segment density

Another measure for the local density of polymer segments along the x–axis is given by the inverse mean distance between neighboring beads in the x–direction. The latter is expressed in terms of the x–projection of the bond vector as $1/\langle Q_k^x\rangle$ which is finite for non-vanishing flow velocities. Since $1/\langle Q_k^x\rangle$ measures roughly the density between beads k and $k+1$ we assign this value to the midpoint between the mean positions of the beads k and $k+1$. We call the density defined this way the quasi–segment density. According to the above the quasi–segment density $\rho'(x)$ is expressed in a form parametrized by the bead index k as

$$\begin{aligned}\rho'_k &= \frac{1}{\langle Q_k^x\rangle}\,, \\ x &= \langle X_{k+1/2}\rangle = \frac{1}{2}\,\langle(X_{k+1}+X_k)\rangle\,.\end{aligned} \tag{49}$$

This definition ensures that ρ' is correctly normalized to N. For comparison with the expression given in Eq. (22) the bead index k must be eliminated from Eq. (49) which can be done explicitly for the Gaussian chain. For this purpose we count the beads starting from the free chain end $k=N$, *i.e.* we transform the bead–index as

$$l = N - j \tag{50}$$

in Eq. (34) and we put the coordinate origin at the free chain end x_0, *i.e.* we use

$$\tilde{x} = x_0 - x \tag{51}$$

as position variable. Then we find from Eq. (39)

$$\langle\tilde{X}_l\rangle = \frac{\beta v b^2}{3}\sum_{i=0}^{l-1} i = \frac{\beta v b^2}{6}\,(l-1)\,l\,. \tag{52}$$

and

$$\tilde{x} = \frac{1}{2}(\tilde{X}_{l+1}+\tilde{X}_l) = \frac{\beta v b^2}{6}\,l^2\,. \tag{53}$$

Solving for l and inserting in Eq. (34) finally yields the ρ' as a function of $\tilde{x}$

$$\rho'(\tilde{x}) = \sqrt{\frac{3}{2\beta v b^2\,\tilde{x}}}\,. \tag{54}$$

Thus the quasi–segment density has the same scaling behavior predicted by the blob model as discussed in section 2.

C Freely jointed chain

In thermal equilibrium Gaussian chains and freely jointed chains show a qualitatively similar behavior [32,31]. However as one can see from Eq. (38) Gaussian chains can be stretched enormously in external fields. Hence we calculate some static properties for the freely jointed chain where the bond length is fixed, too. In equilibrium no orientation is preferred therefore we have

$$P_{eq}(\,\mathbf{Q}_j\,) = \frac{1}{4\pi b^2}\,\delta(\,|\mathbf{Q}_j|-b\,)\,. \tag{55}$$

The flow is taken into account via the Boltzmann factor with the potential in Eq. (30). The conformational distribution function is then given by

$$\begin{aligned}P(\mathbf{R}_0,\{\mathbf{Q}_j\}) &= \delta(\,\mathbf{R}_0\,)\,\frac{1}{4\pi b^2} \\ &\prod_{j=0}^{N-1}\frac{\beta v b\,(N-j)}{\sinh(\,\beta v b\,(N-j)\,)} \\ &\times\delta(|\mathbf{Q}_j|-b)\,\exp(\beta v\,(N-j)\,\mathbf{Q}_j\cdot\hat{\mathbf{x}})\end{aligned} \tag{56}$$

where $\beta=\zeta/k_{\mathrm{B}}T$ as in the preceding section. The first term in this product results from evaluating the partition function and ensures the proper normalization of P.

As for the Gaussian chain we first calculate the first and second moments of the bond vector distribution $P(\mathbf{Q}_k)$ in the presence of flow. We find for the only non-vanishing component of the mean k–th bond vector

$$\begin{aligned}\langle Q_k^x \rangle &= \int d^3\mathbf{R}_0\, d^3\mathbf{Q}_0\, \ldots\, d\mathbf{Q}_{N-1}\, \mathbf{Q}_k \cdot \hat{\mathbf{x}} \\ &\quad \times P(\mathbf{R}_0, \{\mathbf{Q}_j\}) \\ &= \frac{1}{4\pi b^2}\, \frac{\beta v b\,(N-k)}{\sinh(\,\beta v b\,(N-k)\,)} \\ &\quad \times \int d^3\mathbf{Q}_k\, \delta(|\mathbf{Q}_k| - b)\; \mathbf{Q}_k \cdot \hat{\mathbf{x}} \\ &\quad \times \exp(\beta v\,(N-k)\,\mathbf{Q}_k \cdot \hat{\mathbf{x}})\;. \end{aligned} \tag{57}$$

The remaining integral is easily evaluated in spherical coordinates around the x–axis and one obtains

$$\langle Q_k^x \rangle = b\,\mathcal{L}(\,\beta v\,(N-k)\,)\,, \tag{58}$$

where

$$\mathcal{L}(x) = \coth(x) - \frac{1}{x} \tag{59}$$

is the Langevin function. Similarly the only non-vanishing components of the k–th bond covariance are

$$\langle (Q_k^x)^2 \rangle = b^2 \left(1 - 2\,\frac{\mathcal{L}(\,\beta v\,(N-k)\,)}{\beta v\,(N-k)}\right) \tag{60}$$

$$\langle (Q_k^y)^2 \rangle = \langle (Q_k^z)^2 \rangle = b^2\,\frac{\mathcal{L}(\,\beta v\,(N-k)\,)}{\beta v\,(N-k)}\,. \tag{61}$$

As in the previous section all other quantities of interest are easily calculated from these results. In the expression for the mean x–coordinate of the k–th bead

$$\langle X_k \rangle = b \sum_{j=0}^{k-1} \mathcal{L}(\,\beta v\,(N-j)\,)\,, \tag{62}$$

we can replace the sum by an integral and obtain an expression in closed form:

$$\langle X_k \rangle = \frac{1}{\beta v}\, \ln\!\left(\frac{N-k}{N}\, \frac{\sinh(\,\beta v b N\,)}{\sinh(\,\beta v b\,(N-k)\,)}\right)\,. \tag{63}$$

The expressions for the end–to–end distance

$$\begin{aligned}\langle |\mathbf{R}_N - \mathbf{R}_0|^2 \rangle = \quad & b^2 N - b^2 \sum_{j=0}^{N-1} \left(\mathcal{L}(\,\beta v (N-j)\,)\right)^2 \\ & + b^2 \left(\sum_{j=0}^{N-1} \mathcal{L}(\,\beta v (N-j)\,)\right)^2 \end{aligned} \tag{64}$$

and the transverse components of the gyration tensor

$$\begin{aligned} G^{yy} = G^{zz} = \frac{b^2}{2N^2} \sum_{k=0}^{N-1} & (N-k-1)\,(N-k) \\ & \times \frac{\mathcal{L}(\,\beta v\,(N-k)\,)}{\beta v\,(N-k)} \end{aligned} \tag{65}$$

cannot be simplified any further. The results of their numerical evaluation are presented in section 3.

The segment density for the freely jointed chain cannot be brought into an equally simple form as for the Gaussian chain in appendix B.4. However the quasi–segment density introduced in section B.5 is amenable to a semi-analytical treatment. For comparison we again introduce $\tilde{x} = x_0 - x$ and $l = N - j$ to find

$$\tilde{x} = \frac{1}{\beta v}\, \ln\!\left(\frac{\sinh(\beta\, v\, b\, l)}{\beta\, v\, b\, l}\right)\,. \tag{66}$$

To be consistent with the approximation leading to Eq. (63) for $\langle X_l \rangle$ we use $\langle Q_l^x \rangle = X_{l+1} - X_l$ instead of the exact result Eq. (58) to obtain

$$\langle Q_l^x \rangle = \frac{1}{\beta v}\, \ln\!\left(\frac{l-1}{l}\, \frac{\sinh(\beta\, v\, b\, l)}{\sinh(\beta\, v\, b\,(l-1))}\right)\,. \tag{67}$$

For small velocities we have $x_l = \beta v b^2 l^2/6$ and $\langle Q_l^x \rangle = \beta v b^2 l/6$ which is the same as for the Gaussian chain (cf. Eq. (52)).

D Semi-analytical calculations for the FENE spring potential

Instead of using a constraint on the bond lengths like in the previous section a polymer model with a limited extensibility is also obtained if the forces between the segments are described by a potential composed of a repulsive Lennard-Jones potential and an attractive FENE potential [88,97]. Such a potential is also used in the numerical simulations described in appendix E. Here we derive an expression for the end–to–end distance of this model which can be compared with both the results from numerical simulations for this model and with analytical results for the freely jointed chain with a strictly fixed bond length derived in appendix C.

Again the calculation is based on the conformational distribution function like in the previous two appendices; only a different binding potential is used. If the polymer is fixed at one end at $\mathbf{R}_0$ the distribution function reads

$$\begin{aligned} P(\mathbf{R}_0, \{\mathbf{Q}_j\}) = \delta(\mathbf{R}_0)\, \frac{1}{Z} & \\ \times \exp\!\left(-\beta \sum_{j=0}^{N-1} \Phi(\mathbf{Q}_j) + U(\mathbf{R}_j)\right)\,. & \end{aligned} \tag{68}$$

Here the flow potential U is given by Eq. (30) and Z is the partition function. The bond potential Φ is

$$\Phi(\mathbf{r}) = \Phi^{\mathrm{LJ}}(\mathbf{r}) + \Phi^{\mathrm{FENE}}(\mathbf{r})\,, \tag{69}$$

$$\begin{aligned} \Phi^{\mathrm{LJ}}(\mathbf{r}) = 4\epsilon & \left(\left(\frac{\sigma}{|\mathbf{r}|}\right)^{12} - \left(\frac{\sigma}{|\mathbf{r}|}\right)^{6} + \frac{1}{4}\right) \\ & \times \Theta\,(|\mathbf{r}| - R_{\mathrm{LJ}})\,, \end{aligned} \tag{70}$$

$$\Phi^{\mathrm{FENE}}(\mathbf{r}) = -\frac{k_{\mathrm{F}} R_{\mathrm{F}}^2}{2}\, \ln\!\left(1 - \frac{|\mathbf{r}|^2}{R_{\mathrm{F}}^2}\right)\,. \tag{71}$$

The cut–off radius $R_{\rm LJ} = 2^{1/6}\sigma$ is chosen at the minimum of the Lennard–Jones potential and $\Theta(x)$ is the Heaviside function. The other parameters are $k = 30.0$, $R_{\rm F} = 1.5\sigma$ and $\sigma = \epsilon = 1.0$. This results in a minimum of the bond potential at $|\mathbf{r}| = 0.961$.

For the calculation it is useful to introduce spherical coordinates about the x–axis, *i.e.* to let

$$\mathbf{Q}_j = q_j \left(\cos\theta_j, \cos\varphi_j \sin\theta_j, \sin\varphi_j \sin\theta_j\right) . \tag{72}$$

The following integrals appear repeatedly in the calculations

$$\begin{aligned}\mathcal{P}_j^{(p)} &= \frac{\beta v(N-j)}{4\pi} \\ &\int d^3Q_j\, \mathbf{Q}_j^p\, \exp(-\beta\left(\Phi_j - V\hat{\mathbf{x}}(N-j)\mathbf{Q}_j\right)) \\ &= \int_0^\infty dq_j\, q_j^{(p+1)}\, \exp(-\beta\Phi_j)\, \sinh\left(\beta v(N-j)q_j\right) .\end{aligned} \tag{73}$$

Here $\beta = \zeta/k_{\rm B}T$ and p will assume the values $p = 0,\, 1,\, 2$.

The partition function then takes the form

$$Z = \prod_{j=1}^{N-1} \frac{4\pi}{\beta v(N-j)}\, \mathcal{P}_j^{(0)} . \tag{74}$$

For the bond vectors one finds

$$\left\langle |\mathbf{Q}_k|^2 \right\rangle = \frac{\mathcal{P}_k^{(2)}}{\mathcal{P}_k^{(0)}} \tag{75}$$

and

$$\langle Q_k^x \rangle = \frac{\mathcal{P}_k^{(1)}}{\mathcal{P}_k^{(0)}} - \frac{1}{\beta v(N-k)} . \tag{76}$$

This gives for the end–to–end distance

$$\begin{aligned}\left\langle R_E^2 \right\rangle = &\sum_{\substack{j,i=0\\ j\neq i}}^{N-1} \langle Q_j^x \rangle \langle Q_i^x \rangle + \sum_{j=0}^{N-1} \left\langle \mathbf{Q}_j^2 \right\rangle \\ = &\sum_{\substack{j,i=0\\ j\neq i}}^{N-1} \left(\frac{\mathcal{P}_j^{(1)}}{\mathcal{P}_j^{(0)}} - \frac{1}{\beta v(N-j)} \right) \left(\frac{\mathcal{P}_i^{(1)}}{\mathcal{P}_i^{(0)}} - \frac{1}{\beta v(N-i)} \right) \\ &+ \sum_{j=0}^{N-1} \frac{\mathcal{P}_j^{(2)}}{\mathcal{P}_j^{(0)}} .\end{aligned} \tag{77}$$

The results of the numerical evaluation of Eq. (77) are discussed in section 3.

E Bead - spring model for numerical simulations

For the numerical simulations we use the bead spring model as sketched in Fig. 2. Usually one considers the motion on the diffusive time scale only, *i.e.* bead inertia are neglected [98]. The equation of motion for the position of the i–th bead ($i = 1 \ldots N$) is then obtained from a balance between all forces acting on the beads. These forces comprise viscous drag forces $\mathbf{F}^{\rm H}$ on one side and potential– and stochastic forces $\mathbf{F}^{\Phi}$, $\mathbf{F}^{\rm S}$ on the other:

$$-\mathbf{F}_i^{\rm H} = \mathbf{F}_i^{\Phi} + \mathbf{F}_i^{\rm S} . \tag{78}$$

The potential force $\mathbf{F}_i^{\Phi}$ describes the direct interaction between the beads which consists of two contributions: The binding between next–nearest neighbors along the chain is described by one of the two potentials given in Eq. (28) and Eqs. (69)–(71) for the case of harmonic (linear) or anharmonic (nonlinear) springs, respectively:

$$\Phi^{\rm bond} = \sum_{i=0}^{N-1} \Phi^{\rm H}(|\mathbf{R}_{i+1} - \mathbf{R}_i|) \quad \text{or} \tag{79}$$

$$\begin{aligned}\Phi^{\rm bond} &= \sum_{i=0}^{N-1} \Phi^{\rm FENE}(|\mathbf{R}_{i+1} - \mathbf{R}_i|) \\ &= \qquad + \Phi^{\rm LJ}(|\mathbf{R}_{i+1} - \mathbf{R}_i|) .\end{aligned} \tag{80}$$

Here we use an additional bead with index $i = 0$ which is fixed at $\mathbf{R}_0 = 0$ to implement the boundary condition at the tethered chain end. The second contribution comes from the excluded volume effect and acts between any pair of beads. It is described by the repulsive Lennard–Jones potential of Eq. (70),

$$\Phi^{\rm excluded} = \sum_{\substack{i=0\\ j=i+1}}^{N} \Phi^{\rm LJ}(|\mathbf{R}_j - \mathbf{R}_i|) . \tag{81}$$

If excluded volume effects are considered together with nonlinear springs the repulsive part in Eq. (79) is discarded to avoid double counting. If the case without excluded volume effects is under investigation we set $\Phi^{\rm excluded}$ to zero. The potential force $\mathbf{F}_i^{\Phi}$ can thus be calculated as

$$\mathbf{F}_i^{\Phi} = -\nabla_{\mathbf{R}_i} \left(\Phi^{\rm bond} + \Phi^{\rm excluded}\right) . \tag{82}$$

The hydrodynamic forces are [99]

$$\mathbf{F}_i^{\rm H} = -\sum_j \mathsf{H}_{ij}^{-1} (\dot{\mathbf{R}}_j - \mathbf{v}(\mathbf{R}_j)) , \tag{83}$$

where $\mathbf{v}$ is the velocity of the imposed flow and H is the mobility matrix. Without hydrodynamic interactions the mobility matrix is simply diagonal with $\mathsf{H}_{ii} = 1/\zeta$. Hydrodynamic interactions are incorporated in the Oseen tensor approximation [100,32] if desired. This turns the mobility into a conformation dependent tensor which is given by

$$\mathsf{H}_{ij} = \begin{cases} \frac{1}{\zeta}\,1 & \text{for} \quad i = j \\ \Omega(\mathbf{R}_i - \mathbf{R}_j) & \text{for} \quad i \neq j \end{cases} , \tag{84}$$

where

$$\Omega(\mathbf{r}) = \frac{1}{8\pi\eta|\mathbf{r}|} \left(1 + \hat{\mathbf{r}}\hat{\mathbf{r}}^T\right) \tag{85}$$

is the Oseen tensor. Since the Oseen tensor becomes non-positive at small bead separations [33] we always consider the case with hydrodynamic interactions together with the excluded volume effect.

The stochastic forces are related to the dissipative drag by the fluctuation dissipation theorem [101] to ensure the correct equilibrium distribution. We have

$$\mathbf{F}_i^{\mathrm{S}} = \sqrt{2k_{\mathrm{B}}T\,\mathsf{H}^{-1}}\,\xi_i \tag{86}$$

where T is the temperature, k_{B} is the Boltzmann constant and ξ_i is an uncorrelated Gaussian white noise with zero mean:

$$\left\langle \xi(t)\;\xi^T(t')\right\rangle = \delta(t-t')\,1\,. \tag{87}$$

The square root of the mobility tensor H which is responsible for introducing the correlations required by the fluctuation dissipation theorem is calculated approximately by the method of Fixman [102] which is described in detail in appendix F.

To bring these equations into a numerically tractable form we take the positions, velocities, and forces for all beads together as $3N$-dimensional super-vectors $\mathbf{R}$, $\mathbf{V}$, etc. . With a few rearrangements we obtain

$$\mathbf{V} \equiv \dot{\mathbf{R}} = \mathbf{v}(\mathbf{R}) + \mathsf{H}\cdot(-\nabla_{\mathbf{R}}\,\Phi) + \sqrt{2k_{\mathrm{B}}T\,\mathsf{H}}\;\xi\,. \tag{88}$$

Finally we add an artificial inertial term $m\dot{\mathbf{V}}_i$ where the mass is chosen small enough to ensure that momentum equilibration is faster than all the conformational relaxations of the chain. This guarantees that the equilibrium distribution is preserved up to leading order in the integration time step h and allows h to be chosen by a factor of 10 larger than in conventional Brownian dynamics schemes which use the direct discretization of Eq. (88) [77].

The resulting equation is discretized by integration over a small time interval [103] and solved with a velocity–Verlet algorithm [104] as described in more detail in Ref. [77]:

$$\mathbf{R}(t_n+h) = \mathbf{R}(t_n) + \mathbf{V}(t_n)\,h + \frac{h^2}{2m}\,\mathbf{F}(t_n) \tag{89}$$

$$m\mathbf{V}(t_n+h) = m\mathbf{V}(t_n) + \frac{h}{2m}\left(\mathbf{F}(t_n+h) + \mathbf{F}(t_n)\right)$$

$$\mathbf{F}(t_n) = \zeta\left(\mathsf{H}(\mathbf{R}(t_n))\left(-\frac{\partial\Phi}{\partial\mathbf{R}(t_n)}\right) - \mathbf{V}(t_n) + \sqrt{2k_{\mathrm{B}}T\,\mathsf{H}(\mathbf{R}(t_n))}\;\Xi(t_n)\right)$$

The discretized white noise Ξ is now a vector of independent Gaussian random numbers with zero mean and unit variance, *i.e.*

$$\left\langle \Xi(t_n)\;\Xi^T(t_{n'})\right\rangle = \frac{1}{h}\,\delta_{nn'}\,1\,, \tag{90}$$

which can be conveniently generated on a computer.

Several tests of this simulation procedure have been performed under equilibrium conditions as reported in Ref. [77]. One of the test results that is of special relevance to this work is that the effective bond length differs somewhat for the various combinations of interactions that are considered. For the pure Gaussian chain with harmonic springs and no other interactions between the beads the mean square bond length $\langle|\mathbf{Q}|^2\rangle$ at equilibrium is equal to b in Eq. (28) as shown in appendix B.1. The latter is a parameter that can directly be set and we use a value of $b = 1.0$. If excluded volume interactions are added the bond length distribution is distorted and no longer equal to b. An effective bond length b_{eff} can be determined from the equilibrium scaling relation $R_E = b_{eff}N^{3/5}$. The result is $b_{eff} = 1.37$. If the harmonic springs are replaced by FENE springs with the parameters given following Eqs. (69)–(71) the bond length distribution is sharply peaked around the minimum of the potential and one obtains $b = b_{eff} = 0.961$ no matter whether excluded volume interactions is included or not. Finally we mention that the FENE model with excluded volume interactions not only keeps the beads from passing through each other but it also prohibits bond crossings [88,97].

F Efficient evaluation of stochastic forces in the presence of hydrodynamic interaction

A key issue for the present study with emphasis on hydrodynamic interaction is the calculation of the matrix $\sqrt{\mathsf{H}}$ in Eq. (88) and Eq. (89). To make the whole algorithm practical an efficient way to evaluate the square root of the mobility matrix H must be developed. The straight forward calculation of such an expression [105] involves a diagonalization of H which numerically requires an effort of $\mathcal{O}(N^3)$ machine instructions. A second standard method for the calculation of matrix functions is via a series expansion of the desired function [105]. A Taylor series will contain only powers of the matrix argument which are easily evaluated numerically. However, matrix multiplication also requires $\mathcal{O}(N^3)$ operations. A third method which again needs $\mathcal{O}(N^3)$ operations but which offers the most favorable prefactor becomes possible by noting that the square root is not precisely what is needed. Instead one can also use the Cholesky decomposition of H. This idea was exploited in the classic work by Ermak and McCammon [106]. In all cases the numerical effort of $\mathcal{O}(N^3)$ makes the computation prohibitive for long chains. Therefore to our knowledge all previous Brownian dynamics studies of polymer dynamics which took hydrodynamic interactions into account were limited to chains with $N \leq 20$ beads with one exception, the work of Fixman [107], where a few results for a chain of 56 beads are given.

An approximate method which requires only $\sim \mathcal{O}(N^{2.25})$ operations was proposed by Fixman [102]. The starting point for this method is a series expansion of the square root in terms of a complete set of polynomials as in method

two above, *i.e.*

$$\sqrt{\mathsf{H}} = \sum_{\mu=1}^{M} \mathcal{P}^{\mu}(\mathsf{H})\,. \tag{91}$$

A reduction of the computational effort becomes possible by noting that the knowledge of the matrix $\sqrt{\mathsf{H}}$ is actually much more than what is really needed since once it is known it could be applied to *many different* random vectors ξ. For the simulation, however, it needs to be applied to *one single* realization only. A scheme which takes advantage of this is obtained by multiplying both sides of Eq. (91) with ξ. Taking ξ into the sum on the *rhs* one obtains a series expression for $\sqrt{\mathsf{H}}\,\xi$

$$\sqrt{\mathsf{H}}\,\xi = \sum_{\mu=1}^{M} \mathcal{P}^{\mu}(\mathsf{H})\,\xi\,. \tag{92}$$

This expression contains only matrix–vector products and thus its evaluation requires an effort of $\mathcal{O}(N^2)$ only. Furthermore the individual terms in the sum may be calculated recursively keeping the number of these operations low, too.

The polynomials $\mathcal{P}^{\mu}(x)$ may be taken from *any* complete set in function space. The most economic choice are not simple powers $\mathcal{P}^{\mu}(x) = x^{\mu}$ but Chebychev polynomials $C^{\mu}(x)$ [108,109]. These can be evaluated by means of the recursion relation

$$C^{\mu+1}(x) = 2\,x\,C^{\mu}(x) - C^{\mu-1}(x)\,, \tag{93}$$

$$\text{with} \quad C^{1}(x) = x\,,$$

$$\text{and} \quad C^{0}(x) = 1\,. \tag{94}$$

Since the Chebychev polynomials are defined on the interval $[-1,1]$, which is not suitable in the present context, one applies a transformation of the independent variable

$$x = \frac{2y}{b-a} - \frac{b+a}{b-a}\,, \tag{95}$$

which maps the domain of the problem $y \in [a,b]$ to the domain $x \in [-1,1]$ of the Chebychev polynomials. The $C^{\mu}(y)$ appear frequently in numerical analysis and are referred to as shifted Chebychev polynomials [108,109].

If, as in the problem under consideration, the argument x is a matrix, not a simple scalar, then $[a,b]$ is the range of eigenvalues of x. An estimate of the range of the eigenvalues of H is furnished by a simple physical argument: If two nearby beads experience a force in the same direction the induced perturbations of the velocity field will have a large degree of coherence and thus add up to a larger perturbation. If on the other hand the forces are in opposite directions the induced perturbations will cancel out to a large extent. Since beads which are neighbors along the chain are likely to be also close in space an estimate for the largest eigenvalue is obtained by using a force vector with equal forces for all beads as a test-vector $\mathbf{F}$ to form the Rayleigh quotient [105] $\mathbf{F}^T\,\mathsf{H}\,\mathbf{F}/\mathbf{F}^T\,\mathbf{F}$. Similarly an estimate for the smallest eigenvalue is obtained by using a force vector with alternating forces for the beads as a test-vector. To compensate for deviations of these estimates from the true values of the largest and smallest eigenvalues of H one takes a somewhat larger interval for the shifted Chebychev polynomials.

The order of truncation of the series M has to be determined empirically and increases somewhat with N whence the final effort grows with N with a somewhat higher power than 2. To monitor the accuracy of the approximation we compute the exact square root of H via diagonalization using a QR algorithm [105] whenever the conformation is saved. This happens only every 100 - 10000 time steps of the integration and is thus acceptable in terms of computer time.

References

1. J. D. Ferry, *Viscoelastic Properties of Polymers*, 3rd ed. (John Wiley, New York, 1964).
2. P.-G. d. Gennes, *Scaling Concepts in Polymer Physics* (Cornell University Press, Ithaca NY, 1981).
3. R. B. Bird, R. C. Armstrong, and O. Hassager, *Dynamics of Polymeric Liquids, Vol.* 1*: Fluid Mechanics*, 2nd ed. (John Wiley, New York, 1987).
4. H. Giesekus, J. Non-Equilib. Thermodyn. **11**, 157 (1986).
5. R. G. Larson, Rheol. Acta **31**, 213 (1992).
6. R. G. Larson, Rheol. Acta **31**, 497 (1992).
7. U. S. Agarval, A. Dutta, and R. A. Mashelkar, Chem. Engng. Sci. **49**, 1693 (1994).
8. D. V. Boger and K. Walters, *Rheological Phenomena in Focus*, No. 4 in *Rheology Series* (Elsevier, Amsterdam, 1993).
9. J. L. Lumley, Annu. Rev. Fluid Mech. **1**, 367 (1969).
10. P. S. Virk, AIChE J. **21**, 625 (1975).
11. in *Drag Reduction in Fluid Flows*, *Proc. 4th Int. Conf. on Drag Reduction in Bristol*, edited by R. T. Moses and R. H. J. Sellin (Ellis Horwood, Chichester, 1989).
12. in *Structure of Turbulence and Drag Reduction*, *Proc. IUTAM Symp. Zürich 1989*, edited by A. Gyr (Springer, Heidelberg, 1990).
13. A. Gyr and H.-W. Bewersdorff, *Drag Reduction of Turbulent Flows by Additives* (Kluwer Academic Publishers, Dordrecht, 1995).
14. J. P. Hansen and I. R. McDonald, *Theory of Simple Liquids*, 2nd ed. (Academic Press, New York, 1986).
15. J. P. Boon and S. Yip, *Molecular Hydrodynamics* (McGraw-Hill, New York, 1980).
16. D. A. McQuarrie, *Statistical Mechanics* (Harper & Row, New York, 1973).
17. R. G. Larson, *Constitutive Equations for Polymer Melts and Solutions* (Butterworth, Stoneham MA, 1988).
18. R. B. Bird and J. M. Wiest, Annu. Rev. Fluid Mech. **27**, 169 (1995).
19. P.-G. d. Gennes, J. Chem. Phys. **60**, 5030 (1974).
20. E. J. Hinch, Phys. Fluids **20**, S22 (1977).
21. Y. Rabin, F. S. Henyey, and R. K. Pathria, in *Polymer–Flow Interaction*, Vol. 137 of *AIP Conference Proceedings*, edited by Y. Rabin (AIP-Press, New York, 1985).
22. L. G. Leal, in *Structure of Turbulence and Drag Reduction*, edited by A. Gyr (Springer, Heidelberg, 1990).

23. K. S. Schmitz, *An Introduction to Dynamic Light Scattering by Macromolecules* (Academic Press, New York, 1990).
24. V. N. Tsvetkov, in *Newer Methods of Polymer Characterization*, edited by B. Ke (John Wiley, New York, 1964).
25. A. Keller and J. A. Odell, Colloid Polym. Sci. **263**, 181 (1985).
26. K. Walters, *Rheometry* (Chapman & Hall, London, 1975).
27. H. R. Reese and B. H. Zimm, J. Chem. Phys. **92**, 2650 (1990).
28. J. S. Higgins and H. C. Benoît, *Polymers and Neutron Scattering* (Clarendon Press, Oxford, 1994).
29. P. E. Rouse, Jr., J. Chem. Phys. **21**, 1272 (1953).
30. B. H. Zimm, J. Chem. Phys. **24**, 269 (1956).
31. H. Yamakawa, *Modern Theory of Polymer Solutions* (Harper & Row, New York, 1971).
32. M. Doi and S. F. Edwards, *The Theory of Polymer Dynamics* (Clarendon Press, Oxford, 1986).
33. H. C. Öttinger, *Stochastic Processes in Polymeric Fluids* (Springer, Heidelberg, 1996).
34. H. W. Müller and W. Zimmermann, Europhys. Lett. **45**, 169 (1999).
35. W. L. Olbricht, J. M. Rallison, and L. G. Leal, J. Non-Newtonian Fluid Mech. **10**, 291 (1982).
36. A. Onuki, J. Phys. Soc. Jpn. **54**, 3656 (1985).
37. P.-G. d. Gennes, Physica A **140**, 9 (1986).
38. R. B. Bird, R. C. Armstrong, and O. Hassager, *Dynamics of Polymeric Liquids, Vol.* II*: Kinetic Theory*, 2nd ed. (John Wiley, New York, 1987).
39. T. T. Perkins, D. E. Smith, R. G. Larson, and S. Chu, Science **268**, 83 (1995).
40. T. T. Perkins, S. R. Quake, D. E. Smith, and S. Chu, Science **264**, 822 (1994).
41. T. W. Houseal, C. Bustamante, R. F. Stump, and M. F. Maestre, Biophys. J. **56**, 507 (1989).
42. C. Bustamante, Annu. Rev. Biophys. Biophys. Chem. **20**, 415 (1991).
43. S. Chu, Science **253**, 861 (1991).
44. S. Chu, Rev. Mod. Phys. **70**, 685 (1998).
45. R. Pecora, Science **251**, 893 (1991).
46. P. J. Hagerman, Annu. Rev. Biophys. Biophys. Chem. **17**, 265 (1988).
47. S. R. Quake, H. Babcock, and S. Chu, Nature **388**, 151 (1997).
48. S. Manneville *et al.*, Europhys. Lett. **36**, 413 (1996).
49. T. T. Perkins, D. E. Smith, and S. Chu, Science **276**, 2016 (1997).
50. T. T. Perkins, D. E. Smith, and S. Chu, in *Flexible Chain Dynamics*, edited by H. Kausch and T. Nguyen (Springer, Heidelberg, 1997).
51. D. E. Smith and S. Chu, Science **281**, 1335 (1998).
52. D. E. Smith, H. P. Babcock, and S. Chu, Science **283**, 1724 (1999).
53. T. T. Perkins, D. E. Smith, and S. Chu, Science **264**, 819 (1994).
54. D. E. Smith, T. T. Perkins, and S. Chu, Phys. Rev. Lett. **75**, 4146 (1995).
55. P.-G. d. Gennes, Science **276**, 1999 (1997).
56. C. Bustamante, J. F. Marko, E. D. Siggia, and S. B. Smith, Science **265**, 1599 (1994).
57. J. F. Marko and E. D. Siggia, Macromolecules **28**, 8759 (1995).
58. L. Harnau and P. Reineker, New J. Phys. **1**, 3.1 (1999).
59. F. Brochard-Wyart, Europhys. Lett. **23**, 105 (1993).
60. F. Brochard-Wyart, H. Hervet, and P. Pincus, Europhys. Lett. **26**, 511 (1994).
61. F. Brochard-Wyart, Europhys. Lett. **30**, 387 (1995).
62. R. G. Larson, T. T. Perkins, D. E. Smith, and S. Chu, Phys. Rev. E **55**, 1794 (1997).
63. P. Pincus, Macromolecules **9**, 386 (1976).
64. P. Pincus, Macromolecules **10**, 210 (1977).
65. M. Fixman, J. Chem. Phys. **78**, 1594 (1983).
66. B. Dünweg, M. Stevens, and K. Kremer, in *Monte Carlo and Molecular Dynamics Simulations in Polymer Science*, edited by K. Binder (Oxford University Press, Oxford UK, 1995), Chap. 3.
67. H. C. Öttinger, J. Chem. Phys. **86**, 3731 (1987).
68. J. J. Magda, R. G. Larson, and M. E. Mackay, J. Chem. Phys. **89**, 2504 (1988).
69. H. C. Öttinger, J. Chem. Phys. **90**, 463 (1988).
70. R. Rzehak, T. Kawakatsu, D. Kienle, and W. Zimmermann, Partial Draining for a Tethered Polymer in Flow, 1999, to appear in Europhys. Lett.
71. R. Rzehak, T. Kawakatsu, and W. Zimmermann, Relaxation of a Tethered Polymer after Start-up and Cessation of Uniform Flow, 1999, in preparation.
72. R. Rzehak and W. Zimmermann, Using the Karhunen–Loève Method to determine Relaxation Modes and –Times for Nonlinear Polymer Dynamics, 1999, in preparation.
73. M. P. Allen and D. J. Tildesley, *Computer Simulation of Liquids* (Clarendon Press, Oxford, 1987).
74. D. C. Rapaport, *The Art of Molecular Dynamics Simulation* (Cambridge University Press, Cambridge UK, 1995).
75. C. Pierloni and J.-P. Ryckaert, Macromolecules **28**, 5097 (1995).
76. C. Aust, M. Kröger, and S. Hess, Structure and Dynamics of Dilute Polymer Solutions under Shear Flow via Nonequilibrium Molecular Dynamics, to appear inMacromolecules, 1999.
77. R. Rzehak, D. Kienle, T. Kawakatsu, and W. Zimmermann, Brownian Dynamics of Tethered Polymers in Flow, in *Molecular Dynmaics on Parallel Computers*, edited by N. Attig (World Scientific, Singapore, 1999) to appear.
78. J. Hendriks, T. Kawakatsu, K. Kawasaki, and W. Zimmermann, On Semiflexible Polymers in an Anisotropic Medium: A Phenomenological Model, unpublished, 1999.
79. A. Rey, J. J. Feire, and J. Garcia de la Torre, J. Chem. Phys. **90**, 2035 (1989).
80. A. Rey, J. J. Feire, and J. Garcia de la Torre, Macromolecules **24**, 4666 (1991).
81. A. Rey, J. J. Feire, and J. Garcia de la Torre, Polymer **33**, 3477 (1992).
82. J. J. López Cascales and J. Garcia de la Torre, Macromolecules **23**, 809 (1990).
83. J. J. López Cascales, S. Navarro, and J. Garcia de la Torre, Macromolecules **25**, 3574 (1992).
84. K. D. Knudsen, A. Elgsaeter, J. J. López Cascales, and J. Garcia de la Torre, Macromolecules **26**, 3851 (1993).
85. P. J. Flory, *Statistical Mechanics of Chain Molecules* (Interscience Publishers, New York, 1969).
86. W. Kuhn, Kolloid Z. **68**, 2 (1934).
87. H. R. Warner, Jr., Ind. Eng. Chem. Fundam. **11**, 379 (1972).
88. K. Kremer and G. S. Grest, J. Chem. Phys. **92**, 5057 (1990).

89. R. G. Winkler and P. Reineker, Macromolecules **25**, 6891 (1992).
90. D. Kienle and W. Zimmermann, F-shell Blob Model for a Tethered Polymer in Strong Flows, 1999, in preparation.
91. P. Cluzel *et al.*, Science **271**, 792 (1996).
92. S. B. Smith, Y. Cui, and C. Bustamante, Science **271**, 795 (1996).
93. S. B. Smith, L. Finzi, and C. Bustamante, Science **258**, 1122 (1992).
94. J. Happel and H. Brenner, *Low Reynolds Number Hydrodynamics with Special Applications to Particulate Media* (Prentice Hall, Englewood–Cliffs NJ, 1965).
95. J. Leonhard and W. Zimmermann, Deterministic Cross–Streamline Migration of Deformable Objects in Non-uniform Shear Gradients, 1999, in preparation.
96. M. Murat and K. Kremer, J. Chem. Phys. **108**, 4340 (1998).
97. G. S. Grest and K. Kremer, Phys. Rev. A **33**, 3628 (1986).
98. J. D. Schieber and H. C. Öttinger, J. Chem. Phys. **89**, 6972 (1988).
99. R. Zwanzig, Adv. Chem. Phys. **15**, 325 (1969).
100. C. Pozrikidis, *Boundary Integral and Singularity Methods for Linearized Viscous Flow* (Cambridge University Press, Cambridge UK, 1992).
101. H. C. Öttinger and Y. Rabin, J. Rheol. **33**, 725 (1989).
102. M. Fixman, Macromolecules **19**, 1204 (1986).
103. P. E. Kloeden and E. Platen, *Numerical Solution of Stochastic Differential Equations* (Springer, Heidelberg, 1992).
104. H. J. C. Berendsen and W. F. van Gunsteren, in *Molecular Dynamics Simulations of Statistical Mechanical Systems*, edited by G. Ciccotti and W. G. Hoover (North Holland, Amsterdam, 1986), p. 43.
105. G. H. Golub and C. F. v. Loan, *Matrix Computations*, 2nd ed. (John Hopkins University Press, Baltimore MD, 1989).
106. D. L. Ermak and J. A. McCammon, J. Chem. Phys. **69**, 1352 (1978).
107. M. Fixman, Macromolecules **19**, 1195 (1986).
108. A. Björck and G. Dahlquist, *Numerische Methoden*, 2nd ed. (R. Oldenbourg, München, 1979).
109. W. H. Press *et al.*, *Numerical Recipes in C*, 3rd ed. (Cambridge University Press, Cambridge UK, 1990).